Role of the conduction band in electroabsorption, two-photon absorption, and third-harmonic generation in polydiacetylenes

D. Guo and S. Mazumdar
Physics Department, University of Arizona, Tucson, Arizona 85721

S. N. Dixit
Lawrence Livermore National Laboratory, Livermore, California 94550

F. Kajzar
Laboratoire de Physique Electronique des Materiaux, Saclay, F-91191 Gif-Sur-Yvette CEDEX, France

F. Jarka, Y. Kawabe,* and N. Peyghambarian
Optical Sciences Center, University of Arizona, Tucson, Arizona 85721
(Received 8 September 1992)

We report experimental and theoretical investigations of electroabsorption in a polydiacetylene, and determine the complete mechanism of third-harmonic generation (THG) and two-photon absorption (TPA) in linear-chain π-conjugated polymers. The experimental electroabsorption is studied by transmission, rather than reflectance techniques. In addition to the Stark shift of the exciton, a significant feature is observed in the difference spectrum at a higher energy, where the linear absorption is negligible. The origin of this high-energy feature has been controversial. We report several extensive theoretical calculations within the extended Hubbard model, and are able to establish a universality that exists within one-dimensional Coulomb correlated models. We show that the high-energy oscillatory feature in the electroabsorption spectrum originates from the conduction-band threshold, which is separated from the exciton in polydiacetylenes. We also demonstrate that even-parity two-photon states that occur below the one-photon exciton are not observed in electroabsorption due to a cancellation effect. However, a dominant two-photon state that is predicted to occur in between the lowest optical exciton and the conduction-band threshold should be observable. The cancellation, which is only partial for the dominant two-photon state, can, however, reduce the intensity of the resonance due to the state. We show that the conduction-band threshold state, which is an odd-parity one-photon state, also plays an important role in other nonlinear optical processes such as third-harmonic generation and two-photon absorption. Third-order optical nonlinearity in linear-correlated chains is dominated by four essential states: the ground state, the lowest optical exciton and the conduction-band threshold states, and the two-photon state that lies in between the two excited odd-parity states. The two most important predictions of our theoretical work are (a) third-harmonic-generation experiments on ideal isolated strands should find two, not merely one, three-photon resonances, originating from the exciton and the conduction-band threshold states, and (b) only one dominant two-photon resonance in the infinite-chain limit should be observable in THG and TPA. Extensive comparisons between theoretical predictions and experiments are made to prove the validity of the theory. Conjugated polymers other than the polydiacetylenes are discussed briefly.

I. INTRODUCTION

Organic π-conjugated polymers with large optical nonlinearities and short excited-state relaxation times have generated considerable recent interest as potential optoelectronic materials.[1-4] Recent work by several groups[5-7] have suggested potential practical uses, although it is also being realized that an order-of-magnitude increase in nonlinearities and/or figures of merit would be necessary for commercial applications. In particular, it has been pointed out that a large intensity-dependent refractive index in organics is usually accompanied by a strong two-photon absorption that is detrimental to switching applications.[8,9] Clearly it is of interest to theoretically and experimentally determine the role of two-photon absorption *vis-à-vis* other nonlinear processes in order to attain enhanced nonlinear effects.

Several different techniques have been employed to identify the mechanism of nonresonant optical nonlinearity in the organics. Third-harmonic generation (THG),[9-14] degenerate four-wave mixing (DFWM),[15,16] and electric-field-induced second-harmonic generation (EFISH) (Refs. 17 and 18) have been the most popular among these. These experiments, and the accompanying theoretical work,[19-22] have emphasized the role of a dominant above-gap two-photon state. Additional insight into the electronic structures of these systems is also obtained from electroabsorption studies,[23-30] in which the photoabsorption is measured in the presence of a static electric field applied parallel to the chain. New in-

0163-1829/93/48(3)/1433(27)/$06.00

duced optical transitions become allowed in the presence of the applied electric field, and it is expected that a detailed analysis of the induced transitions can give us valuable information on the underlying electronic structure as well as nonlinear optical processes.

In the present paper we focus on a specific polydiacetylene, (poly[1,6-di(*N*-carbazolyl)-2-4-hexadiyne]) (DCH-PDA), for which we have performed electrotransmittance. A detailed theoretical analysis is done, within the context of an extended Hubbard model, treating the field-induced effect in a nonperturbative manner. Brief presentations of our work have been made previously.[30] Our approach finds that the low-energy two-photon states that occur below the exciton in the π-conjugated polymers play no role in electroabsorption or optical nonlinearity. On the other hand, we find that the conduction-band edge plays a very strong role in the electroabsorption, and we are able to resolve a basic controversy[23-27] that has persisted in the literature. Furthermore, we have also determined that the conduction-band edge plays an equally important role in other third-order nonlinear optical processes.[30] The importance of the band edge was not understood before this work, and it is our belief that thereby a three-photon resonance in the THG of PDA's has previously been incorrectly identified as two-photon resonance due to an even-parity state that occurs below the lowest optical exciton.[10,12,20]

In the past, electroabsorption studies have been performed for a number of π-conjugated polymers,[23-29] as well as σ-conjugated polymers such as the polysilanes.[31,32] Here we limit ourselves to the PDA's, in which it has been argued that the optical gap is dominated by Coulomb interaction,[33] although electron-phonon interactions play a non-negligible role and give rise to vibronic sidebands in the linear absorption spectrum. The nature of the electroabsorption in *trans*-polyacetylene[28,29] is quite different from that in the PDA's. We will therefore discuss π-conjugated polymers other than the PDA's only briefly, pointing out both the similarities and the differences. Similarly, the very strong dimerization in the polysilanes requires a somewhat modified theoretical description, and this will be discussed elsewhere.[34] We focus on a crystalline PDA here, in order to develop a complete understanding of the behavior of the isolated linear strand. Our reasons for choosing DCH-PDA are twofold. First, this system possesses a well-defined conduction gap, and has a sharp excitonic feature in its absorption spectrum, in contrast to several other PDA's that are either disordered or exhibit thermochromism and photochromism. Second, significant progress has been made in the fabrication of oriented organic thin films of DCH-PDA that are of high optical quality.[17,35]

In Sec. II, we present the experimental details of our work. The electroabsorption is studied by transmission, rather than reflectance measurements, for several different electric fields, both parallel and perpendicular to the chain axis. In agreement with previous works[23-26] on PDA's, we conclude that both the linear absorption and the electroabsorption originate from the PDA backbone. Also in agreement with previous works, we find that the Stark shift of the exciton is accompanied by a second high-energy feature, in a region where linear absorption is negligible. While this feature of the electroabsorption has been noted before, its interpretations differ. Sebastian and Weiser ascribed the origin of the high-energy signal to dipole-allowed transitions to the conduction band.[23,24] Later work by Tokura and co-workers[25,26] and Hasegawa *et al.*,[27] however, have concluded that this feature originated from a dipole-forbidden two-photon state that becomes weakly allowed in the presence of the symmetry-breaking electric field. Since the dominant role of a two-photon state above the lowest optical state has been emphasized in all theoretical investigations of third-order optical nonlinearity,[19-22] it is clearly of interest to determine the precise origin of the high-energy feature in the electroabsorption spectra. Our transmission study very clearly indicates the high-energy feature to be oscillatory about zero, rather than occurring as peaks. Based on the accompanying theoretical work, we conclude that such an oscillatory signal can arise only from the conduction band, with participation by both allowed and forbidden states within the band.

In Sec. III, we present our theoretical work, which is carried out both for the noninteracting Su-Schrieffer-Heeger (SSH) model[36] and for interacting electron cases within the framework of an extended Hubbard model. Important symmetry relations found within the SSH model persist in the correlated case and are used to predict weak participation in electroabsorption by low-energy two-photon states that occur within the optical gap. For zero Coulomb correlations, the theoretical electroabsorption spectrum is easily calculated. Generating the electroabsorption spectrum for nonzero Coulomb interactions is, however, nontrivial. Investigation of Coulomb correlation effects (which are accurate enough to generate two-photon states below[37] the lowest optical state) require numerical calculations in rather short chains, which have discrete spectra, and lack a true conduction band. Furthermore, the numerical calculations give total energies, and the number of total-energy states even for relatively short chains is quite large. As has been recently shown by us,[22] the techniques that are used for obtaining the energies of low-lying states in the infinite chain from $N \rightarrow \infty$ extrapolations of finite-chain data are not appropriate for high-energy states. Thus there is no simple way to determine the precise conduction-band edge from the energies alone. We resolve this problem by combining exact finite-chain numerical calculations and a physical intuitive picture based on the valence bond (VB) theory of correlated systems. For readers unfamiliar with the valence bond notation, we present in Appendix A a discussion of the natures of the exciton, conduction band, and biexciton wave functions in the VB basis. We first calculate the energy of the conduction-band edge as well as the electroabsorption for extremely large Coulomb interaction parameters, where the energy manifolds containing the exciton states, the conduction band, and the biexciton states are all well separated, and the conduction-band edge can be determined from energy considerations alone. We then examine the wave functions corresponding to the conduction-

band states, and determine several different techniques to identify conduction-band states from wave-function characteristics. These techniques involve calculations of various transition dipole moments and correlation functions. These same techniques are then used to determine the conduction-band edge in the case of intermediate as well as small Coulomb interactions. It is found that a well-defined universality exists within the extended Hubbard Hamiltonian, such that the methods used to locate the conduction band in the strong correlation limit carry over to the case of moderate to small correlations, where energy considerations fail to locate the conduction-band edge. The electroabsorption calculations, for both strong and intermediate Coulomb interactions, find a high-energy oscillatory feature in the difference spectrum beginning precisely from the conduction-band edge identified by the wave-function analysis discussed above. A dominant two-photon state with unusually large dipole coupling with the exciton is located between the exciton and the conduction-band edge. In linear chains with a bond-order wave ground state, this two-photon state can be close to the exciton in energy,[21,22] and causes a peak in the theoretical difference spectrum. We believe that such a feature appears in the experimental difference spectrum. However, this evidence is not yet conclusive. To a large extent this is attributed to the relatively small energy difference between the exciton and the conduction-band edge, and the prominence of the electroabsorption signals caused by the band states. Further complication arises from the fact that in this same frequency region the vibrational sideband is seen in the linear absorption, and this should have its own field-induced energy shift. One other important conclusion of our theoretical work is that the well-known two-photon states that occur *below* the exciton[37] in short polyenes will not be observable in the electroabsorption difference spectrum. This is because of a cancellation effect that we discuss qualitatively in Sec. III. A more quantitative discussion is given in Appendix B.

From our theoretical work we have determined that the conduction-band edge also plays a strong role in THG processes. This role is discussed in Sec. IV. Earlier works on third-order optical processes[19–22] have focused on the role of a specific above-gap two-photon state that has unusually strong dipole coupling with the lowest optical exciton. We show here that the threshold state of the conduction band is a one-photon-allowed odd-parity state that is located above the dominant two-photon state, and that the dipole moment between these latter pairs of states is nearly as large as that between the exciton and the dominant two-photon state. In addition to the two previously known[19–21] nonlinear optical channels that include only the ground state, the exciton, and the two-photon state, we identify a third very important channel that involves all of the above states and the conduction-band threshold state of odd parity.[30] We discuss the one-to-one correspondence between this and the theoretical description of the third-order optical process in the noninteracting limit of zero Coulomb correlation,[38,39] where each two-photon state is equally strongly dipole coupled to *two* one-photon states placed symmetrically below and above it. Nonzero Coulomb correlations lead to unequal energy splittings between the two one-photon states and the dominant two-photon exciton, while maintaining strong (but unequal) dipole couplings between them. We have briefly shown elsewhere[30,40,41] how these four "essential states" can be used to develop a phenomenological model of optical nonlinearity in the organics that can successfully explain THG and direct two-photon absorption (TPA) spectra. Here we point out that the implication of our work is that *two* distinct three-photon resonances are expected in THG measurements in the PDA's, a strong one at one-third the energy of the exciton, and a weaker one at one-third the energy of the band edge.[30,40,41]

In Sec. V, we make comparisons between theoretical predictions and experiments. While we focus mostly on electroabsorption, we also discuss THG and TPA, and, in particular, the occurrence of the second three-photon resonance in THG. Experimentally, the second three-photon resonance has already been observed in PDA's, but, in the past, this has often been incorrectly assigned to a two-photon resonance[9,10,20,35] due to an even-parity state located below the lowest optical state. For cases where both THG and TPA data exist,[12,40] it is found from energy considerations alone that the higher-frequency resonance in the THG spectrum does not originate from a two-photon state. Furthermore, from a theoretical analysis of intensities, we show that two-photon resonances due to these low-energy even-parity states should have vanishing intensities in long chains.[41,42] The present conclusion, viz. that the high-frequency resonance in THG is a three-photon resonance, resolves this issue.

The theoretical results obtained by us can be summarized as follows. In Fig. 1, we have shown schematically the states that we will be most concerned with. The $1B_u$ is the lowest optical exciton, below which several low-energy two-photon states can occur. Only the lowest of these, the $2A_g$, is included in the figure. These low-energy two-photon states contribute very weakly to optical nonlinearity, because of a cancellation effect. The mA_g in the figure is the dominant two-photon state that has very large dipole coupling with the $1B_u$, and is expected to contribute a peaklike structure in the electroabsorption spectrum. We do not discuss the location of the mA_g in detail, as it has been previously shown that it occurs between the $1B_u$ and the $2B_u$ excitons for all Coulomb interactions and chain lengths.[21,22] The conduction band begins from the threshold odd-parity state nB_u, and consists of closely spaced A_g and B_u states. States at the conduction-band edge give rise to an oscillatory feature in the electroabsorption spectrum. The oscillation originates from the increased transition probability to the zero-field-forbidden A_g states and the decreased transition probability to the zero-field-allowed B_u states. Third-order optical nonlinearity, in the presence of moderate to strong Coulomb interactions, is determined almost entirely[30] by the four essential states, the $1A_g$, $1B_u$, mA_g, and nB_u.

Finally, we emphasize that although much of the quan-

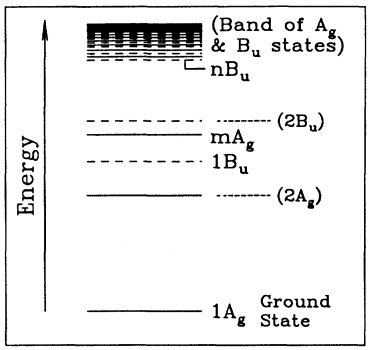

FIG. 1. The schematic of the energy levels in a one-dimensional Coulomb correlated chain. Only A_g states that have the same electron-hole symmetry as the ground state, and B_u states that have opposite electron-hole symmetries, are shown. The $1A_g$, $1B_u$, mA_g, and nB_u are the "essential states" that we argue will dominate third-order optical nonlinearity. While we show only one A_g state below the $1B_u$, it is conceivable that several other such states exist in this region. These are the nonessential states whose contribution to third-order optical nonlinearity is extremely weak, and perhaps even vanishing in the infinite chain due to a cancellation effect. The contribution by the mA_g does not vanish because it is dipole coupled to B_u states ($1B_u$ and nB_u) that are of different nature: the $1B_u$ is an exciton, the nB_u is the conduction-band threshold state.

titative information here is obtained from finite-chain calculations, our interest lies in determining the proper results for the infinite chain. In each of the cases studied here we have verified the chain-length independence of the locations of the essential states by performing calculations for chain lengths $N=4$, 6, 8, and occasionally 10 for literally hundreds of parameters.

II. EXPERIMENTS

We have chosen DCH-PDA for our experiments because it readily forms long parallel chains and can be synthesized into a thin film made of small single crystals using vacuum deposition techniques.[17,35] Our sample was prepared in the manner outlined in Refs. 17 and 35. The monomer form of the sample was deposited on a potassium hydrogen phthalate substrate, giving small single crystals within the 400-Å film. The polymer was then formed using thermal energy by baking the monomer at 150 °C for 24 h. We were able to confirm the unidirectional polymer-chain alignment by observing the varying transmission of polarized light through the sample as the angle was changed between the polarization axis and the chain axis.

The linear absorption of our sample with light polarized along the chain axis is shown in Fig. 2. The large absorption peak at 1.85 eV is attributed to an exciton, since photoconductivity is absent in this energy region. The photoconductivity threshold occurring at around 2.4 eV supports this assignment.[43] The observed photoconduction band is not visible in the linear absorption spectrum. Because of the strong oscillator strength of the exciton, the conduction band has a weak oscillator strength and is enveloped by the high-energy tail of the exciton peak. Closer inspection of this tail reveals a series of smaller peaks which are vibronic absorption peaks caused by phonon absorption coupled with the exciton.[44] Because of the extremely strong peak absorption coefficient of the exciton, 2×10^5 cm^{-1}, earlier researchers have done electroreflectance measurements on bulk samples. The high-quality thin films obtained by using the processing techniques of Refs. 17 and 35 allow us to do transmission measurements.

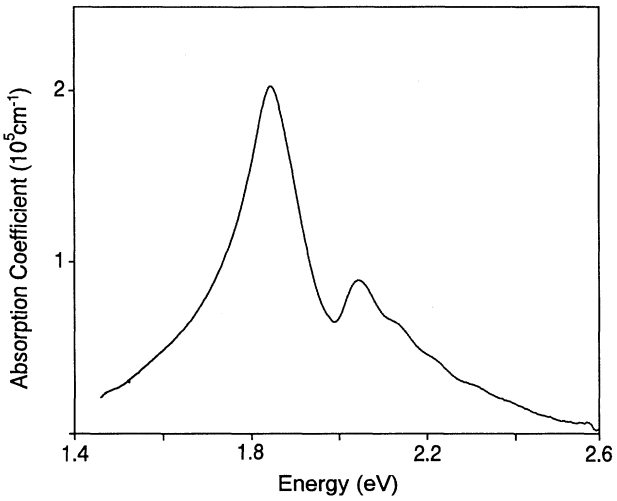

FIG. 2. Linear absorption in DCH-PDA.

In order to apply an electric field to our sample, aluminum electrodes were deposited so that the electric field between the electrodes would be parallel to the molecular chain (the direction in which the electron experiences maximum delocalization). We used a 50-μm wire mask to obtain the electrode spacing that would allow strong fields without a need for extremely high voltages. A quick calculation shows that with this gap and desired fields above 100 kV/cm, we must apply voltages in excess of 500 V. To switch these voltages on the sample for signal detection with a lock-in amplifier, we constructed a transistor switching circuit with an input from a pulse generator. This gave a 200-Hz rectangular unipolar field with the four applied field strengths, 60, 80, 100, and 120 kV/cm, where we observed arcing on the sample above 120 kV/cm.

Our light source was a halogen lamp powered by a homemade 12-V feedback-stabilized dc power supply utilizing four lead-acid batteries. We use the lamp filament at the entrance slit to a monochromator which acted as a narrow-band filter for the light incident on the sample. A photomultiplier tube was placed after the sample and the signal was processed by an EG&G lock-in amplifier and collected by a computer. We were able to scan from 1.46 to 2.76 eV, being limited by the photomultiplier tube (PMT) cutoff at low energy and the light source output at high energy.

The electric-field-induced differential absorption was obtained from the measured differential transmission.

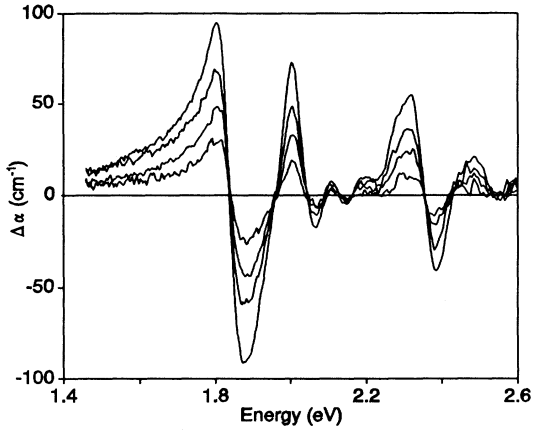

FIG. 3. The electric-field-induced difference spectrum in DCH-PDA for fields of 60, 80, 100, and 120 kV/cm. The differential absorptions were obtained from transmission measurements.

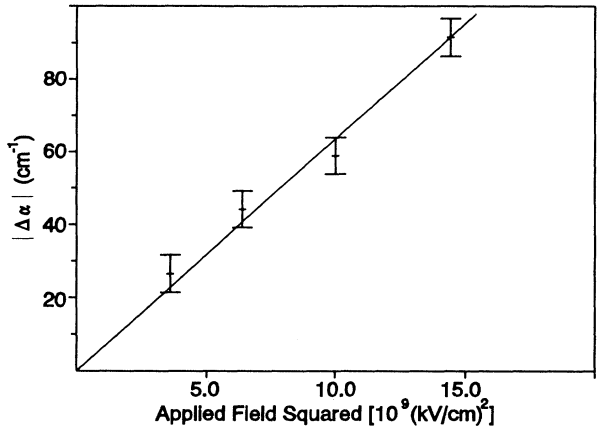

FIG. 5. The Stark shift of the exciton vs the square of the applied field.

Figure 3 shows the differential absorption $\Delta\alpha$ for the four applied field strengths. Comparison with the linear absorption of Fig. 2 indicates that the low-energy feature between 1.8 and 2.1 eV originates from a redshift of the exciton and its vibronics in the $\Delta\alpha$ spectrum. This is confirmed by comparing the derivative spectrum of the linear absorption with the actual experimental $\Delta\alpha$ spectrum. The derivative spectrum is obtained in the usual manner, by rigidly shifting the linear absorption and taking the difference between the spectrum induced by the highest field and the field-free spectrum. The computed derivative spectrum is then subtracted from the experimental difference spectrum for comparison. The results of this comparison are shown in Fig. 4, which clearly indicates that the electroabsorption structure in the vicinity of the exciton energy is a simple Stark shift of the exciton. The exciton shift is plotted against the square of the applied field F in Fig. 5, where we see that the shift increases linearly with F^2, indicating a true Stark shift. Furthermore, the presence of a peak on the immediate high-energy side of the exciton at about 2 eV in Fig. 4 suggests that this feature is related to a field-induced absorption to the one-photon-forbidden state mA_g (see Fig. 1) that becomes weakly allowed in the presence of the applied field. We postpone further discussion of this peaklike feature until Sec. V, where we compare theoretical results with experiments.

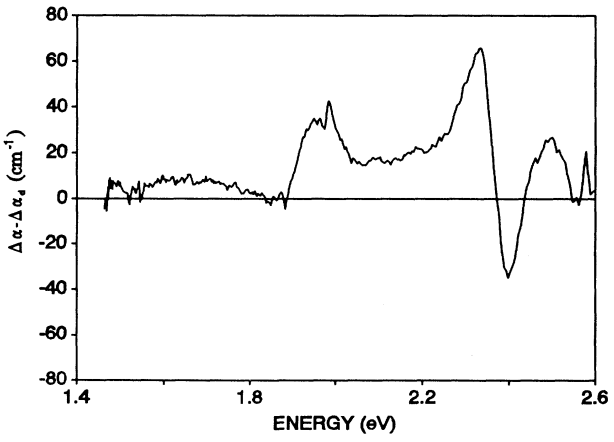

FIG. 4. The difference between the observed electroabsorption spectrum $\Delta\alpha$ for a field of 120 kV/cm and the derivative spectrum $\Delta\alpha_d$ of the linear absorption in Fig. 2. It is conceivable that the peaklike structure at about 2 eV originates from the field-induced absorption due to the mA_g (see text).

In addition to the Stark shift of the exciton and the peaklike structure at 2 eV in Fig. 3, the electroabsorption difference spectrum also shows a high-energy oscillatory signal starting from around 2.35 eV. The occurrence of this signal in Fig. 4 indicates that it does not result from a mere shift of the linear absorption, but is an entirely different field-induced feature. It is this signal that has attracted the attention of earlier investigators.[23–27] The signal crosses zero several times, indicating both positive and negative field-induced contributions. This is significant, as the theoretical work presented in Sec. III shows that states which are one-photon allowed in the absence of the field make negative contributions to the differential absorption, while previously one-photon-forbidden but two-photon-allowed states make positive contributions. We show theoretically that the oscillation requires a continuum composed of both allowed and forbidden states. Thus the high-energy feature arises from the conduction-band states of the PDA, and it is not a coincidence that the photoconductivity threshold is at the same energy.[43]

III. THEORY OF ELECTROABSORPTION

Prior to the work by the present authors,[30] the only theoretical work in the area of electroabsorption in the organics that we are aware of was based on a phenomenological model,[45] and dealt with the Stark shift of the exciton in a donor-acceptor charge-transfer solid. Comparisons of experimental electroabsorption spectra with

theory have therefore largely involved predictions obtained within theories valid for conventional inorganic semiconductors.[46] While similarities do exist between the electroabsorptions in conventional inorganic and organic semiconductors, the mechanisms of linear absorptions are quite different, absorption in the conjugated polymers being mediated by charge transfer between π orbitals centered on different carbon atoms. For proper comparison to experiments in π-conjugated polymers, it is necessary to evaluate the electroabsorption within an appropriate theoretical model. In order to elucidate the mechanism of electroabsorption in the PDA's, we first discuss the theory of electroabsorption for the simple case of a dimerized band of noninteracting electrons. This is then followed by a more realistic theory within extended Hubbard models, which include the electron-electron Coulomb interactions that lead to exciton formation.

It should be emphasized that electroabsorption, like THG and TPA, may be treated as a third-order nonlinear optical process and can be obtained from calculating $\chi^{(3)}(-\omega;\omega,0,0)$. However, this particular nonlinear phenomenon can also be calculated within a nonperturbative approach that gives directly the total field-induced change in absorption as well as energy shifts. This is achieved by constructing a Hamiltonian matrix whose basis consists of the eigenfunctions of the field-free Hamiltonian, with the electric-field term contributing to off-diagonal matrix elements between the basis functions. There are two advantages of this procedure. First, it is valid for any arbitrary field strength, and in principle, can be used for calculating strong-field effects[23,24] (although in practice it is not possible to calculate strong-field effects in short finite chains). Second, this has been the conventional approach in the case of inorganic semiconductors,[46] and following the same approach can therefore allow comparisons between the theories of conventional semiconductors and the PDA's.

A. Electroabsorption within the noninteracting model

We consider the dimerized Hückel model (SSH model with fixed dimerization)

$$H_{\text{Hückel}}=t\sum_{i,\sigma}(1\pm\delta)(c_{i,\sigma}^{+}c_{i+1,\sigma}+c_{i+1,\sigma}^{+}c_{i,\sigma}) , \tag{1}$$

where $c_{i,\sigma}^{+}$ creates a π electron of spin σ at carbon atom (hereafter, site) i, t is the nearest-neighbor hopping integral, and δ a bond-alternation parameter. Strictly speaking, the above model is applicable only to *trans*-polyacetylene, and description of the PDA's should involve three different hopping integrals to mimic the superalternation characteristic of those systems with both double and triple bonds. Even when this superalternation is included, however, strong optical transition occurs only from the highest occupied states to the lowest unoccupied states. Thus only relatively unimportant quantitative differences are obtained by including a third hopping integral, while making the actual numerical computations unnecessarily complicated. We can therefore neglect this aspect without loss of essential features of the electroabsorption.

The boundary condition we assume is that of an open chain with an even number of atoms. Eigenstates of even linear-chain polyenes are either of even parity (hereafter A_g) or of odd parity (hereafter B_u) with respect to the center of inversion. In addition, the Hamiltonian in Eq. (1) has electron-hole symmetry, and the A_g and B_u states are further characterized by their electron-hole symmetries. We shall be interested only in the A_g states that have the same electron-hole symmetry as the ground state, and B_u states that have the opposite electron-hole symmetry. The total-energy states are constructed out of the single-particle band orbitals that are obtained as the solutions to Eq. (1). Each state is further characterized by a principal quantum number that gives its relative ordering within the A_g or the B_u subspace. The dipole operator is written as

$$\mu=\sum_{i}\left[\frac{N+1}{2}-i\right](n_i-1) , \tag{2}$$

where $n_i=\sum_\sigma c_{i,\sigma}^{+}c_{i,\sigma}$ is the total number operator corresponding to site i, and N is the number of sites. The symmetry of the dipole operator allows one-photon transitions only between A_g and B_u states of opposite electron-hole symmetries. This is the reason for retaining only A_g and B_u states of appropriate electron-hole symmetries. The ground state consists of completely filled single-particle valence-band levels, and is therefore necessarily of A_g symmetry. This is the $1A_g$ state. Optically allowed dipole transitions from the ground state therefore are to the B_u states, while transitions to the excited A_g states are one-photon forbidden but two-photon allowed.

Charge conjugation symmetry within Eq. (1) implies that there is a conduction-band level at $+\epsilon$ corresponding to each single-particle valence-band orbital at $-\epsilon$. The symmetry characteristics of the band levels are perfectly alternating, so that optical transition from the filled valence-band level at $-\epsilon$ to the conduction-band level at $+\epsilon$ is dipole allowed. In addition to these "symmetric" transitions, additional "asymmetric" transitions from even (odd) parity valence-band levels at $-\epsilon$ to odd-(even-) parity conduction-band levels at $+\epsilon'$ ($\epsilon'\neq\epsilon$) are also weakly allowed in short chains. In long chains, however, only the symmetric transitions are important. In Fig. 6, we show that the transition dipole moments corresponding to typical symmetric transitions increase with the chain length N, while the strengths of the "asymmetric" transitions, after reaching a peak, actually decrease with N, and become vanishingly small in the long-chain limit. This is not surprising, because for $N\rightarrow\infty$ the symmetric transitions in a linear chain correspond to the momentum-conserving transitions in a periodic ring, and the differences between the periodic and the open boundary cases are expected to vanish. This limitation to symmetric transitions will be important in our discussions of electroabsorption and optical nonlinearity.

The above is the standard description for linear absorption. Within perturbation theory, a weak static electric field F applied parallel to the chain direction can

significantly alter this description by mixing the A_g and B_u states according to

$$|n\rangle = |n^{(0)}\rangle + \sum_{m \neq n} \frac{\langle n^{(0)}|H_F|m^{(0)}\rangle}{E_n^{(0)} - E_m^{(0)}} |m^{(0)}\rangle \ . \tag{3}$$

Here $H_F = \mu F$ is the perturbation introduced by F. The unperturbed wave functions and energies are denoted by $|n^{(0)}\rangle$ and $E_n^{(0)}$, while $|n\rangle$ represents the perturbed wave function.

It should be noted that Eq. (3) does not necessarily imply participation of A_g states in electroabsorption. We illustrate this with the case of a typical A_g state, the $2A_g$ (the very high-energy A_g states that occur at twice the optical gap and are reached by promoting two electrons across the optical gap are not being considered here). The $2A_g$ is coupled to the only two B_u states that are reached through symmetric transitions, the $1B_u$ and the $2B_u$. In Fig. 7(a), we show the orbital occupancies for the $1A_g$, $1B_u$, $2A_g$, and $2B_u$ states for arbitrary N. Figure 7(b) displays the total energies corresponding to these states. Only the highest two occupied orbitals and the lowest two unoccupied orbitals are shown in Fig. 7(a). According to Fig. 6, the B_u states that are reached by unsymmetric transitions are irrelevant, even though their dipole moments with the $2A_g$ is nonzero for short chains. From Eq. (3), the perturbed $2A_g$ state is

$$|2A_g\rangle = |2A_g^{(0)}\rangle + \frac{\langle 2A_g^{(0)}|H_F|1B_u^{(0)}\rangle}{E_{2A_g}^{(0)} - E_{1B_u}^{(0)}} |1B_u^{(0)}\rangle + \frac{\langle 2A_g^{(0)}|H_F|2B_u^{(0)}\rangle}{E_{2A_g}^{(0)} - E_{2B_u}^{(0)}} |2B_u^{(0)}\rangle \ . \tag{4}$$

The ground state is essentially unperturbed by the electric field because of the large optical gap. Absorption from the ground state to the perturbed $2A_g$ state is weakly allowed in the presence of nonzero field, the transition dipole moment between the ground state and the perturbed $2A_g$ being given by

$$\langle 1A_g^{(0)}|\mu|2A_g\rangle = \frac{\langle 2A_g^{(0)}|H_F|1B_u^{(0)}\rangle}{E_{2A_g}^{(0)} - E_{1B_u}^{(0)}} \langle 1A_g^{(0)}|\mu|1B_u^{(0)}\rangle + \frac{\langle 2A_g^{(0)}|H_F|2B_u^{(0)}\rangle}{E_{2A_g}^{(0)} - E_{2B_u}^{(0)}} \langle 1A_g^{(0)}|\mu|2B_u^{(0)}\rangle \ . \tag{5}$$

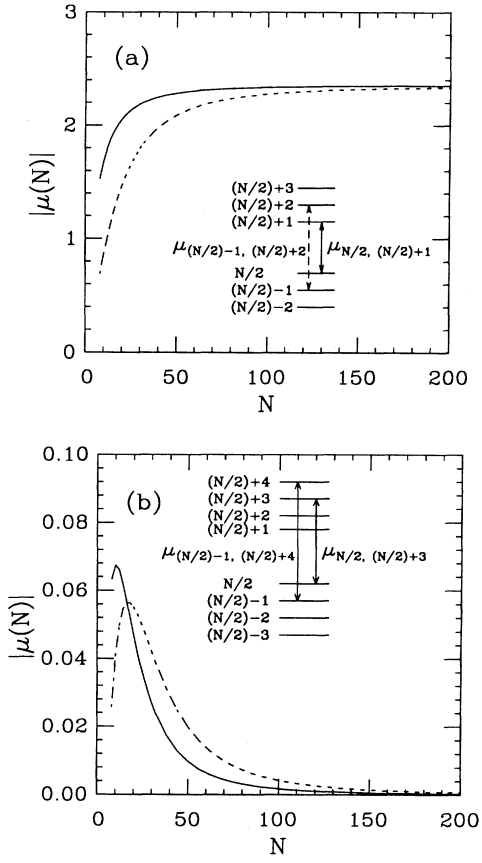

FIG. 6. The transition dipole couplings corresponding to transitions between single-particle valence- and conduction-band levels that are (a) symmetrically placed with respect to the chemical potential, and (b) asymmetrically placed with respect to the chemical potential. Only the symmetric transitions are important for the infinite chain, so that while considering the contribution of any intraband A_g state to optical nonlinearity, only two intraband B_u states need be considered.

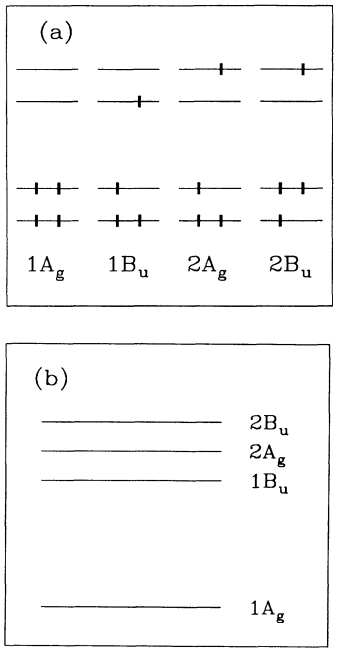

FIG. 7. (a) The occupancies of the single-particle band levels for the $1A_g$, $1B_u$, $2A_g$, and $2B_u$ states. Only the highest two valence-band levels and the lowest two conduction-band levels are shown. (b) The total energies of the four states. The energy difference between the $2A_g$ and the $1B_u$ states is the same as that between the $2B_u$ and the $2A_g$.

Since for all N, $E^{(0)}_{2B_u} - E^{(0)}_{2A_g} = -(E^{(0)}_{1B_u} - E^{(0)}_{2A_g})$, it might appear that the contributions involving the $1B_u$ and $2B_u$ can lead to cancellation in the infinite-chain limit, where $\langle 1A_g^{(0)}|\mu|1B_u^{(0)}\rangle = \langle 1A_g^{(0)}|\mu|2B_u^{(0)}\rangle$. This is, however, not true, since the numerators of the two terms in the right-hand side of Eq. (5),

$$\langle 1A_g^{(0)}|\mu|1B_u^{(0)}\rangle\langle 1B_u^{(0)}|\mu|2A_g^{(0)}\rangle$$

and

$$\langle 1A_g^{(0)}|\mu|2B_u^{(0)}\rangle\langle 2B_u^{(0)}|\mu|2A_g^{(0)}\rangle ,$$

are of opposite signs. This property can be proved by writing the $|1B_u^{(0)}\rangle$, $|2B_u^{(0)}\rangle$ and $|2A_g^{(0)}\rangle$ as Slater determinants and evaluating the relevant matrix elements of μ. Instead of cancellation, the two terms on the right-hand side of Eq. (5) contribute in an additive manner, and intraband A_g states should contribute strongly in electroabsorption. This is opposite to the case of THG, where from very similar reasoning it has been shown[41,42] that the two-photon resonance due to the $2A_g$ has a vanishing intensity in the $\chi^{(3)}$ spectrum in the infinite noninteracting chain.

Notice that the additive contribution is true only for the uncorrelated case. For nonzero Coulomb correlation, the lowest A_g states (for, e.g., the $2A_g$) can occur below[37] the $1B_u$, and, for the two B_u states to which they are coupled, the corresponding energy denominators in Eq. (5) will have the same sign, while the numerators in the two terms on the right-hand side of Eq. (5) continue to have opposite signs and nearly equal magnitudes (see Appendix B). Therefore subgap A_g excitations will not be observable in electroabsorption spectra owing to the near cancellation between the contributions by the two B_u states.

From Eq. (3), contributions to the electroabsorption by B_u and A_g states are of opposite signs. For $F \neq 0$, intensities of transitions from $1A_g$ to B_u states decrease, while previously forbidden A_g states become weakly allowed. Figure 8 shows the electroabsorption spectrum of a noninteracting chain of 100 atoms. The oscillatory electroabsorption signal results from the A_g and B_u states that are very close to one another in the band. In the infinite chain with a true continuum, the high-frequency oscillations deep within the band will disappear due to cancellation, but the band-edge signal would persist. The noninteracting model cannot give the exciton seen in the PDA's and is not appropriate for comparison with experiments.

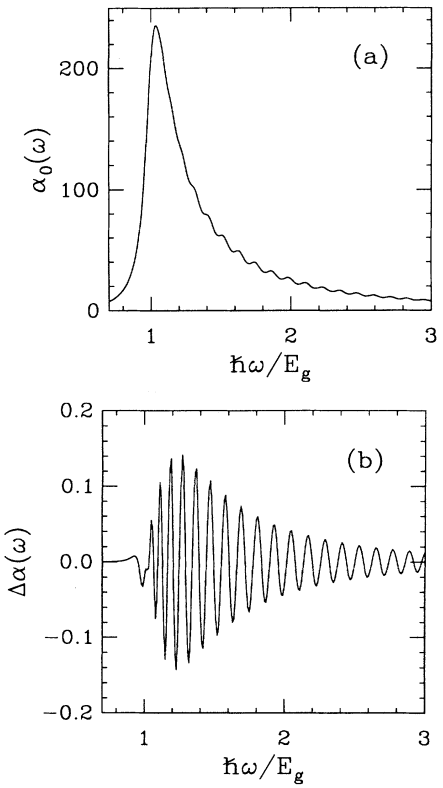

FIG. 8. (a) The calculated linear absorption in arbitrary units for a Hückel chain of $N=100$, $\delta=0.2$; (b) The calculated electric-field-induced difference spectrum, in arbitrary units, for the same chain for a dimensionless field $F=0.00008$. The oscillations deep inside the band are due to finite size, and will vanish in the true infinite chain, but the band-edge signal would persist.

B. Electroabsorption within interacting Hamiltonians

The SSH model predicts a broad band-to-band optical transition, and cannot explain the excitonic absorption in the PDA's. Inclusion of the direct Coulomb interaction between the electrons is essential for properly describing the optical properties of the PDA's.[3] We model this with an extended Hubbard Hamiltonian,

$$H_{EH} = H_{\text{Hückel}} + U\sum_i n_{i,\uparrow}n_{i,\downarrow} + V\sum_i (n_i - 1)(n_{i+1} - 1) . \quad (6)$$

Here $n_{i,\sigma} = c^+_{i,\sigma}c_{i,\sigma}$, $n_i = \sum_\sigma n_{i,\sigma}$, U is the Coulomb repulsion between two electrons occupying the same π orbital, and V is the nearest-neighbor Coulomb interaction. A simple Hubbard model ($V=0$) can give an optical gap E_g dominated by the Coulomb interaction, but does not give rise to exciton binding,[33] and hence is not discussed in this paper. We shall impose the restriction $U > 2V$, since for $U < 2V$ it is known that the ground state is a charge-density wave (CDW) with on-site modulation of the charge densities.[33] We neglect intersite interactions beyond the nearest neighbor, because, for the very short chains we are dealing with, it is difficult to reproduce continuumlike behavior with longer-range Coulomb interactions.

We emphasize that the above theoretical description does not include the role of electron-phonon interaction. This is because even for reasonable chain lengths it becomes intractable to treat both electron-electron and electron-phonon interactions simultaneously. The complexity increases further when investigating nonlinear optics, because we have to consider the entire energy spectrum in principle. Our motivation here is to arrive at a *qualitative* understanding of the electronic states that

dominate the nonlinear optical channels in the Coulomb correlated PDA's.[33] This is not to suggest that electron-phonon interactions play no role in the PDA's. Rather, we take the view here that electron-phonon interactions can give rise to vibrational sidebands, but not to distinct electronic states whose characters are different from the solutions of the electronic Hamiltonian alone. This approach has been shown to lead to excellent qualitative descriptions of the ground states and low-energy excitations in PDA's.[33]

There exists no analytical approach for accurate calculations of excited states within Eq. (6). The only available technique involves numerical calculation of both the linear absorption and the electroabsorption. Unfortunately, however, numerical calculations within Eq. (6) are necessarily limited to rather short chains. It then becomes necessary to generate the features associated with a continuum from finite-chain calculations, even though finite chains have discrete spectra. This can be tricky, especially for realistic U, V, and F. On the other hand, it is known that for artificially large Coulomb correlations the "intraband" gaps are small even for small N, and the spectrum begins to resemble that of long chains. Our approach is then as follows. We first present the results of the electroabsorption calculation for very large U and V, where the exciton and conduction-band states are well separated and analysis of the nature of the states contributing to the electroabsorption is simple. Since the conduction-band threshold state is easily identifiable here, detailed analysis of the corresponding wave function is possible. In this manner, the characteristics of the wave function corresponding to the conduction-band threshold state are determined. Then, for intermediate to weak Coulomb correlations, all wave functions are tested against these predicted characteristics to determine the lowest conduction-band state. We will demonstrate that the results of our calculations are quite universal, and the expected pattern of behavior is the same even for realistic U and V.

We will therefore initially treat the case in the strongly correlated $U>2V\gg t$ regime of Eq. (6). For what follows, it is useful to physically understand the $t=0$ energy spectrum, which remains qualitatively correct even for $|t|>0$. It should be kept in mind that we use a total-energy scheme, and not single-particle states. We use the term "band" loosely to describe collections of states that have zero gap between them in the infinite-chain limit. On the other hand, the term "conduction band" will have the usual meaning, referring to states with delocalized particle and hole (where the particle and hole are defined below). For $V=0$, the spectrum consists of $(N/2)+1$ "bands," centered at 0, U, $2U$, . . . , $(N/2)U$. For $V>0$, all of the above bands, except the lowest one (which consists of covalent spin-wave states), are further split. This may be understood from the typical real-space many-electron configurations shown in Fig. 9 (see also Appendix A). States which occurred at U for $V=0$ are split into exciton states at $U-V$ and band states at U. The excitons consist of real-space configurations with a doubly occupied site (hereafter, particle) and an empty site (hereafter, hole) as nearest neighbors, while the particle and the hole are separated from each other in the conduction-band states. Within Eq. (6) the particle and the hole are free to separate as soon as the distance between them is more than one lattice constant, and thus all such configurations constitute the conduction band. The band that is at $2U$ for $V=0$ consists of configurations with two particle-hole pairs, and the band splittings for $V>0$ are much more complicated. In this case, it is possible to have levels at $2U-3V$, $2U-2V$, $2U-V$, $2U$, $2U+V$, and $2U+2V$. Examples of configurations which have these energies at $t=0$ are included in Fig. 9. States at $2U-3V$ are called biexcitons, while the other states with two double occupancies consist of separated excitons.

Configurations	Energy at t=0
↑ ↑↓ ↑↓ ↓ ∘ ∘ ↑ ↓	2U+2V
↑↓ ↑ ↓ ∘ ∘ ↑ ↑↓ ↓	2U+V
↑↓ ↑ ∘ ↓ ↑↓ ↑ ∘ ↓	2U
↑↓ ↑ ∘ ↑↓ ↓ ∘ ↑ ↓	2U−V
↑↓ ↑ ∘ ↑↓ ∘ ↓ ↑ ↓	2U−2V
↑ ↑↓ ∘ ↑↓ ∘ ↓ ↑ ↓	2U−3V
↑ ↑↓ ↓ ↑ ∘ ↓ ↑ ↓	U
↑ ↓ ↑↓ ∘ ↑ ↓ ↑ ↓	U−V
↑ ↓ ↑ ↓ ↑ ↓ ↑ ↓	0

FIG. 9. Typical many-electron real-space configurations and their energies in the limit of zero hopping.

For $|t|>0$ the above description remains valid, except that considerable overlap can occur between the various energy manifolds, the overlaps increasing with t/V and t/U. In particular, the overlaps between the conduction-band states at U and biexciton states at $2U-3V$ can be rather large if the only restriction one has is $U>2V$. In order to minimize such overlaps and to correctly identify the origin of high-energy electroabsorption, we initially show the results of our electroabsorption calculation for U, $V\gg t$, and $U>3V$. Intermediate and weak correlation cases are discussed subsequently.

Case 1: Strong Coulomb interactions, $U=50, V=15$

The specific U and V which we have chosen are $U=50$ and $V=15$, where $t=1$. Exact numerical calculations for zero and nonzero fields were performed for $N=8$, which has $485\,A_g$ and $460\,B_u$ states. Since nonzero F mixes the A_g and B_u subspaces, the overall dimension of the Hamiltonian matrix for $F\neq 0$ is 945. For $N=10$ the overall dimension of the Hamiltonian matrix increases by an order of magnitude, but the spectrum still remains discrete. This is about the largest system whose entire energy spectrum can be analyzed by exact calculations. Thus numerical calculation for $N>8$ would require considerably larger amount of effort, without giving additional physical insight. In order to simulate the behavior of the infinite chain, therefore, we work with large U and V to generate the continuum at U, and also employ artificially

large dc fields to simulate the energy shifts and the $\Delta\alpha$ and α of the infinite chain. We emphasize that the evaluation of the electroabsorption did not involve the perturbation expression in Eq. (3). Rather, the exact A_g and B_u eigenstates and the dipole moments between them are first evaluated for $F=0$. These dipole moments are then used to determine the off-diagonal matrix elements in the total Hamiltonian for $F\neq 0$, whose basis space consists of the eigenstates of the field-free Hamiltonian. Diagonalization of the new Hamiltonian gives the exact solution for $F\neq 0$. Optical absorptions are separately calculated for the two cases of zero and nonzero fields to obtain the differential absorption.

Before we present the numerical results for the electroabsorption, it is useful to analyze the solutions of the field-free (but nonzero t) case, from which the nonzero-field results can be anticipated. In Fig. 10, we have shown the energy spectrum, up to and including energy levels centered at $2U-2V$. Higher-energy levels cannot participate in electroabsorption, because their dipole couplings to the lowest B_u states is zero. It is clearly seen that for such large values of U and V the different kinds of states are well separated by sizable energy gaps, and therefore the identification of individual states (as spin wave, exciton, band, etc.), necessary to analyze the theoretical electroabsorption spectrum, is simple. For example, there is a distinct gap between the $29A_g$, the highest exciton state, and the $20B_u$, the lowest conduction-band state. The energy gap between the highest conduction-band state centered at $U(86A_g)$ and the lowest biexciton state centered at $2U-3V(77B_u)$ is also visible. What will be most relevant in this context are the quantum number and the energy of the state that forms the lower threshold of the conduction band, which we hereafter refer to as the nB_u. For the very large U and V considered here, $n=20$ for $N=8$. This can be understood in the context of valence bond theory, as illustrated in Appendix A. The B_u subspace does not have any covalent valence bond diagram. The number of exciton states is simply the number of singly ionic valence bond basis functions in which a double occupancy and an empty site occur as nearest neighbors. There are 19 such B_u functions in $N=8$, and therefore as many B_u exciton states. For smaller U and V, n could be smaller than 20. For considerably smaller U and V, the distinction between exciton and conduction-band states becomes fuzzy in short chains. The quantum number n increases with U and V until an N-dependent saturation value is reached, where the saturation value depends on the number of possible excitonic B_u states. For $N=4$, 6, 8, and 10, the saturation values for n are 3, 7, 20, and 67, respectively. This saturation behavior is analogous to the saturation behavior of the quantum number of the mA_g that is strongly dipole coupled to the $1B_u$ (Ref. 21).

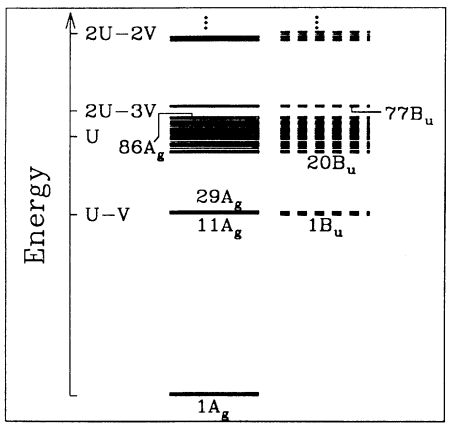

FIG. 10. The energy spectrum for $N=8$, $U=50$, $V=15$, $t=1$, and $\delta=0.1$. There are ten spin-wave states. Notice the large energy gap between the $29A_g$, the highest exciton state, and the $20B_u$, the lowest conduction-band state. Levels at $2U-3V$ are biexcitons. The relatively large width of the conduction band is explained in Appendix A.

From Eq. (3) it is clear that a strong mixing for nonzero field occurs between those A_g and B_u states which are very close in energy and which are very strongly dipole coupled. We therefore consider the transition dipole matrix elements between pairs of states both of which lie within the same energy manifold. The number of excitonic A_g states ($11A_g$–$29A_g$) is the same as the number of B_u excitons, viz. 19. We have examined in detail the transition dipole moments between each pair of A_g and the B_u excitonic states. In Table I, we present the energies of the various excitonic A_g states and their transition dipole moments with $1B_u$. Obviously, the $11A_g$ is unique in having a very strong dipole moment with the $1B_u$, while all other dipole moments are smaller by at least one order of magnitude. Indeed, the dipole moment between $11A_g$ and $1B_u$ is much larger than even that between the $1A_g$ and $1B_u$. This is to be expected, given that the $1B_u$ and $11A_g$ states both occur in the exciton band, while the $1A_g$–$1B_u$ transition is across the much larger optical gap. Very similar results are obtained when the dipole moments with the excitonic $2B_u$ are considered, the only difference being that the $2B_u$ is very strongly dipole coupled to the next higher A_g exciton, viz. the $12A_g$. Once again, this particular feature, very strong dipole coupling between each excitonic B_u

TABLE I. Energies of the A_g excitons and their transition dipole moments with the $1B_u$ exciton for $N=8$, $U=50$, $V=15$, and $\delta=0.1$. The $1B_u$ exciton occurs at energy 34.8624. The dipole moments are to be compared with $|\langle 1A_g|\mu|1B_u\rangle| = 0.1265$. The A_g states with quantum numbers between 15 and 28 have transition dipole moments smaller than $\langle 14A_g|\mu|1B_u\rangle$ and are not shown.

Quantum number j of A_g exciton	Energy	$\langle jA_g\|\mu\|1B_u\rangle$
11	35.1190	0.9945
12	35.1820	0.1056
13	35.2192	−0.1108
14	35.2362	0.0035
⋮	⋮	⋮
29	35.6705	0.0003

state and a unique A_g exciton, is common[21,22] to all U and V. The quantum number m of the mA_g state which has strong dipole coupling with the $1B_u$ increases with U (beginning from $m=2$ for $U=0$), until it reaches an N-dependent saturation value. For the example we have chosen here, m has already reached its saturation value of 11. Elsewhere we have shown[21,22] that the energy of the mA_g is close to that of the $1B_u$ exciton for arbitrary U and V. The proximity of the mA_g to the $1B_u$ and the large dipole coupling between them suggest that the mA_g would participate strongly in electroabsorption, leading to a redshift of the $1B_u$ exciton.

The transition dipole moments between the conduction-band states are even larger than those between exciton levels. Starting from the $20B_u$, each conduction-band level is very strongly dipole coupled to *two* other conduction-band states of opposite symmetry. This feature is identical to the behavior of the nonin-

TABLE II. Transition dipole moments between conduction-band states for $N=8$, $U=50$, $V=15$, and $\delta=0.1$. Only the strong transition moments are shown. Notice that the magnitudes of these dipole moments are larger than or comparable to $|\langle 11A_g|\mu|1B_u\rangle|=1.2651$ and other dipole moments between exciton states. Here $E(jB_u)$ and $E(kA_g)$ are energies of the corresponding states in units of t.

Quantum number j of B_u states in conduction band	Quantum number k of A_g states in conduction band	$E(jB_u)$	$E(kA_g)$	$\langle jB_u\|\mu\|kA_g\rangle$
20	30	46.8840	46.8845	4.1885
	35		48.0819	−1.1098
21	31	47.0411	47.0415	4.2155
	36		48.1863	−1.1168
22	32	47.1967	47.1970	4.1899
	37		48.2946	−1.0978
23	33	47.3176	47.3179	4.1984
	38		48.3757	−1.1016
24	34	47.7391	47.7395	3.6128
	43		49.0222	0.6482
	44		49.4283	−0.6180
25	30	48.0812	46.8865	−1.1134
	35		48.0819	4.6209
26	31	48.1857	47.0415	−1.1011
	36		48.1863	4.6459
27	32	48.2940	47.1970	−1.1011
	37		48.2946	4.6120
28	33	48.3752	47.3179	−1.1047
	38		48.3757	4.6277
29	39	48.3898	48.3902	3.1493
	49		49.7545	0.8217
⋮	⋮	⋮	⋮	⋮
70	80	52.7979	52.7982	4.4707
	85		53.7375	1.1238
71	81	52.8956	52.8959	4.4596
	86		53.8719	−1.1156
⋮	⋮	⋮	⋮	⋮
75	80	53.7374	52.7982	1.1249
	85		53.7375	4.1176
76	81	53.8718	52.8959	−1.1170
	86		53.8719	4.0858

teracting band states. The strong dipole moments within the band are larger than even $\langle mA_g|\mu|1B_u\rangle$. This is shown in Table II, where we have listed representative states at both the lower and upper thresholds of the conduction band. The behavior of intermediate-band states that are not included in Table II are identical, *viz.* each A_g state is very strongly coupled to two B_u states and vice versa. The dipole moments in Table II should be compared with $\langle 1A_g|\mu|1B_u\rangle$, which is only -0.1265. We emphasize that while only the transition dipole moments whose magnitudes are larger than 0.6 are listed in Table II, each conduction-band state also has moderate dipole couplings (where "moderate" is arbitrarily defined to be those with magnitudes greater than twice $|\langle 1A_g|\mu|1B_u\rangle|$) with several other conduction-band states of opposite symmetry. Both these features of conduction-band states, viz. extraordinarily large dipole couplings with two neighboring states, and moderate couplings with several other band states, distinguish them from excitonic A_g or B_u states. Furthermore, these are also the characteristics of the noninteracting band. The complete dipole-moment calculations are summarized in Fig. 11, where the sudden jump in dipole moments beginning from a well-defined threshold is clearly discernible. From the very large transition dipole matrix elements within the band, as well as the very small energy differences between the corresponding levels, one expects that the mixing between the A_g and B_u conduction-band states is much stronger than that between the exciton states.

From Eq. (2), the large transition dipole moments between conduction-band states is a signature of greater particle-hole separation in these states as compared to that in the exciton states. We have calculated correlation functions $1/N\langle \sum_i (n_i-1)(n_{i+l}-1)\rangle$ as a function of the separation l. The correlation function is the joint expectation value that the sites i and $i+l$ are occupied by particles (double occupancies) or holes (empty sites). For example, if the correlation function is positive for a given pair of sites, it implies that either both sites are occupied by particles, or both are occupied by holes. A negative correlation function implies that one of the sites is occupied by a particle, the other by a hole. In Table III, we show these correlation functions for representative spin-wave, exciton, conduction-band, and biexciton states. The exciton states of both A_g and B_u symmetries are characterized by small particle-hole separations that result in the large values for the correlation functions at $l=1$ but the very small values at larger l. Note the sudden jump in the particle-hole separation, as evidenced by larger values of the correlation function at larger l, beginning from $20B_u$ and extending all the way up to $86A_g$, which is the highest conduction-band state. This behavior of the correlation functions indicates delocalized particle and hole. The biexciton character of wave functions beginning from the $77B_u$ should also be clear. Here we have two real-space excitons, with particles and holes alternating. The signs of the density-density correlation functions should therefore be alternating (with the nearest-neighbor correlation function being negative), and the magnitudes of the first three terms are expected to have the ratio 3:2:1.

Having characterized the conduction-band wave functions, we calculate the linear absorption and the electroabsorption. In Fig. 12, the linear absorption for $U=50$ and $V=15$ is shown. As a result of the very large V, the oscillator strength of the linear absorption is almost totally concentrated in the $1B_u$ exciton. This feature is only quantitatively modified for smaller Coulomb interactions and in longer chains, where moderately strong intensities can be expected for transitions to other low-lying B_u excitons. In Fig. 13(a), we show the difference absorption spectrum for dimensionless field $F=0.005$, corresponding to about 900 kV/cm, assuming a mean lattice constant of $1.4A$ and $t=2.5$ eV. As anticipated, the shift of the $1B_u$ exciton is to the red. The second positive peak in Fig. 13(a), close to the exciton, corresponds to the mA_g. No other exciton A_g state is visible. A_g states that occur below the $1B_u$ are not observable, and this is not merely

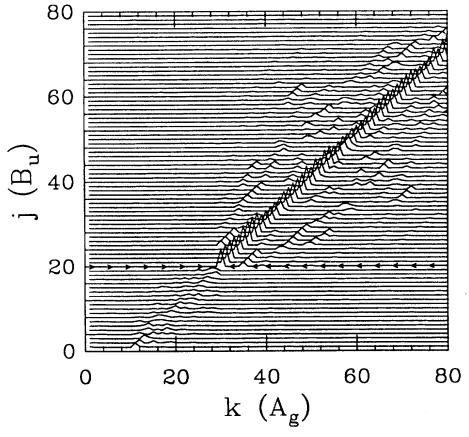

FIG. 11. The three-dimensional plot of the magnitudes of the transition dipole moments between the A_g and B_u states for $N=8$, $U=50$, $V=15$, $t=1$, and $\delta=0.1$. The vertical heights correspond to the magnitudes of the dipole moments. Notice the threshold behavior of the $20B_u$.

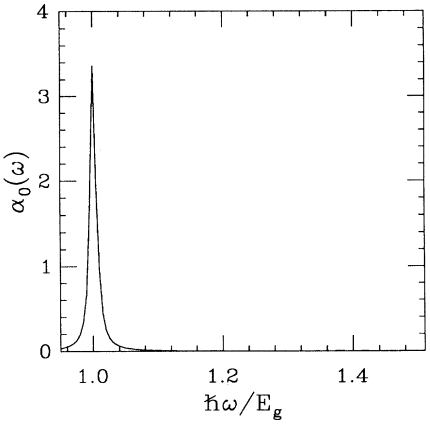

FIG. 12. The calculated linear absorption in arbitrary units in a $N=8$ chain for the parameters of Figs. 10 and 11. A finite half-width of $0.05t$ has been included in our calculation of the spectrum.

TABLE III. Expectation values $1/N\langle \sum_{i=1}^{N-1}(n_i-1)(n_{i+l}-1)\rangle$ as a function of l for $N=8$, $U=50$, $V=15$, and $\delta=0.1$. A large negative value implies a strong particle-hole correlation. The numbers with magnitudes smaller than 0.001 are listed as 0.

	States		l = 1	2	3	4	5	6	7
Covalent	$1A_g$		−0.002	0	0	0	0	0	0
	⋮		⋮	⋮	⋮	⋮	⋮	⋮	⋮
	$10A_g$		0	0	0	0	0	0	0
	$1B_u$		−0.128	0.002	−0.002	0	0	0	0
	⋮		⋮	⋮	⋮	⋮	⋮	⋮	⋮
	$19B_u$	Exciton	−0.125	0	−0.002	0	0	0	0
	$11A_g$		−0.128	0.003	−0.002	0	0	0	0
	⋮		⋮	⋮	⋮	⋮	⋮	⋮	⋮
	$29A_g$		−0.124	0	0	0	0	0	0
Band	$20B_u$		−0.006	−0.006	−0.029	−0.038	−0.030	−0.015	0.004
	⋮		⋮	⋮	⋮	⋮	⋮	⋮	⋮
	$76B_u$		−0.004	−0.009	−0.030	−0.038	−0.029	−0.013	0.003
	$30A_g$		−0.006	−0.006	−0.029	−0.038	−0.030	−0.015	0.004
	⋮		⋮	⋮	⋮	⋮	⋮	⋮	⋮
	$86A_g$		−0.004	−0.009	−0.030	−0.038	−0.029	−0.013	0.004
	$77B_u$		−0.345	0.227	−0.123	0.001	−0.001	0	0
	⋮		⋮	⋮	⋮	⋮	⋮	⋮	⋮
	$82B_u$		−0.338	0.221	−0.120	−0.001	0	0	0
	⋮	Biexciton	⋮	⋮	⋮	⋮	⋮	⋮	⋮
	$87A_g$		−0.345	0.227	−0.123	0.001	−0.001	0	0
	⋮		⋮	⋮	⋮	⋮	⋮	⋮	⋮
	$92A_g$		−0.338	0.221	−0.120	−0.001	0	0	0

because their dipole couplings with the $1B_u$ are weak. Rather, cancellations of the kind discussed in Sec. III A minimize contributions by subgap A_g states to electroabsorption (see below and Appendix B). In addition to the features near the optical gap E_g, an oscillatory signal occurs from $1.345E_g$. The high-energy oscillatory signal is shown more clearly in the inset in Fig. 13(a). Note the absence of linear absorption in this energy region in Fig. 12. From the energies of the states shown in Fig. 10, it is unambiguous that the threshold of the oscillatory signal is the conduction-band threshold state $20B_u$. As discussed above, this oscillation is a result of contributions to the difference spectrum by both A_g and B_u states. This is further demonstrated in Fig. 13(b), where the contributions to the electroabsorption by the A_g and B_u states are plotted separately. We emphasize that the results of Fig. 13(b) were obtained by exact solution of the full Hamiltonian containing both A_g and B_u bases. The A_g and B_u contributions are separated only in the calculations of the linear absorption coefficients α's. Note that the vertical scale in Fig. 13(b) is giant compared to the inset in Fig. 13(a), indicating huge contributions to $\Delta\alpha$ by individual conduction-band A_g and B_u states. The very large individual contributions by the conduction-band A_g and B_u states result both from giant transition dipole moments as well the small intra-conduction-band energy gaps. It is conceivable that in the case of a true continuum at $N\rightarrow\infty$, one large broad feature would be obtained for conduction-band states of a given symmetry. The overall difference spectrum is obtained by summing the contributions from the respective A_g and B_u states, so that deep inside the band one expects a true cancellation. At the band edge, however, there exist states only on the high-energy side, and the oscillation survives here.

The above results can be summarized as follows. The $1B_u$ is coupled more strongly to the mA_g than to the $1A_g$. This leads to a redshift of the $1B_u$ exciton for $F\neq 0$. The mA_g leads to a peak in the difference spectrum, close to the $1B_u$ exciton. The contribution to the electroabsorption by A_g states that occur below the $1B_u$ is negligible, because of the cancellation effect. The conduction-band threshold states, while participating weakly in linear absorption, give rise to an observable oscillatory signal in the difference spectrum, which is the sum of giant contributions of opposite signs by states of opposite symmetries. While we show the results for only $N=8$, identical results are obtained[47] also for $N=4$ and 6, the only difference being larger discreteness and smaller n for smaller N. We have verified that the behavior is also identical for other strong Coulomb interaction parameters (e.g., $U=23$, $V=6$; $U=20$, $V=6$). For large N, a true continuum starting from nB_u is expected. The very large U and V allows us to determine unequivocally the different kinds of energy states within the field-free energy spectrum even for finite N, as well as to obtain a difference spectrum with prominent features that are well separated.

We have, in the above, pointed out three distinct ways

of identifying the band threshold state nB_u: (i) it is the lowest state whose energy is linear in U (rather than $U-V$); (ii) transition dipole moments between neighboring states become noticeably larger starting from this particular state: and (iii) as with the transition dipole moment, a sudden jump occurs in particle-hole separation at the conduction-band threshold. Since the energy gaps at moderate U and V become fuzzier, and since the quantum number n of the B_u state that forms the lowest conduction-band state is arbitrary for these U and V, we point out here a fourth means of identifying this state: the mA_g also has a strong dipole coupling[42] with the nB_u. This aspect of the nB_u will be discussed in the case 2 subsection.

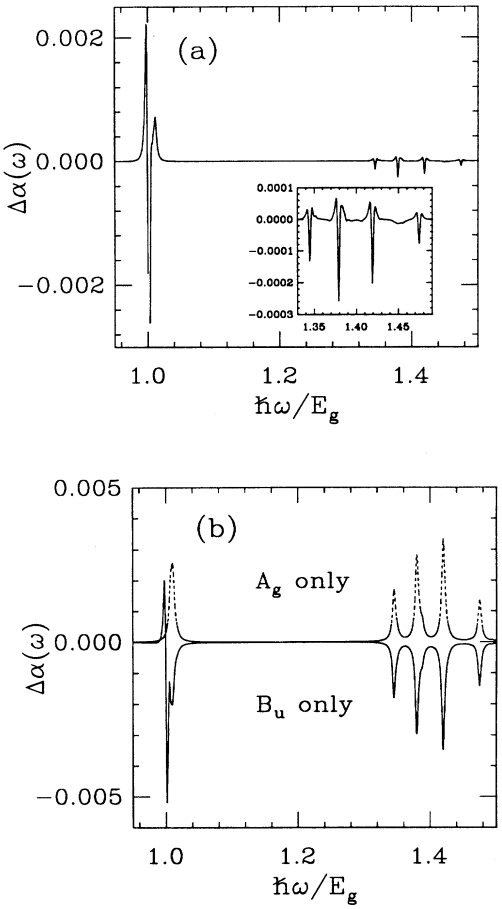

FIG. 13. (a) The calculated electric-field-induced ($F=0.005$ in dimensionless units) difference spectrum, in arbitrary units, for $N=8$ and the parameters of Figs. 10 and 11. The inset shows the high-energy features due to the conduction band, with the scale magnified. Note the shapes of the individual features, indicating splitting of levels very close in energy, rather than simple shifts of B_u states. (b) The individual contributions by A_g and B_u states to the electroabsorption difference spectrum. The units are the same in (a). Notice that the vertical scale is larger than the inset in (a) by an order of magnitude. The electroabsorption in (a) is a sum of the contributions by A_g and B_u states.

Case 2: Moderate Coulomb interactions, $U=10, V=3$

Our motivation is to demonstrate the universality of the theoretical results for even moderate Coulomb interactions. We now discuss the results for the representative case of $U=10$ and $V=3$. These particular U and V were chosen for the following reasons. The value of U and $U-V$ are large enough that the ground state is still dominated by covalent valence bond wave functions, while the value of V is large enough to have exciton binding even in this chain length ($N=8$). On the other hand, since the value of V is moderate, there is considerable overlap between the exciton "band" and the conduction band. The total energies of the very highest exciton states, defined as states with localized particle-hole interaction, can be actually above those of the lowest conduction-band states, defined as those in which the particle and the hole are free. Similar overlaps also occur between the conduction band and the biexciton states. All these are shown schematically in Fig. 14(a). Thus the correlation parameters chosen are truly intermediate. Care should therefore be taken in the interpretation of the theoretical data, as the quantum numbers of the conduction-band A_g and B_u states do not increase monotonically at the band threshold.

The exact energy spectrum is shown in Fig. 14(b) for

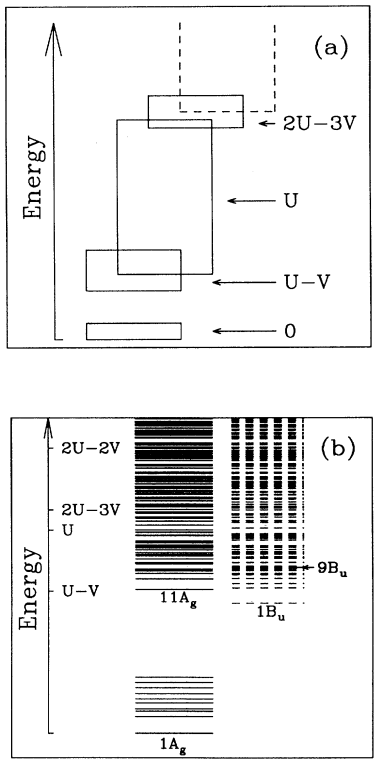

FIG. 14. (a) Schematic of the spin-wave "band," the exciton "band," the conduction "band," and the biexciton "band" for intermediate Coulomb interactions. (b) The energy spectrum for $N=8$, $U=10$, $V=3$, and $t=1$, $\delta=0.1$. The $9B_u$ is the conduction-band threshold state from the wave-function analysis (see text).

this case, where we have indicated the mA_g ($m=11$) and the specific B_u state that is determined to be the conduction-band threshold state nB_u ($n=9$). Note that identification of the $9B_u$ as the conduction-band threshold state would not be possible from energy considerations. We employ all the criteria discussed in the case 1 subsection to identify the lowest conduction-band state. It is shown that all of these identify the same B_u state as the conduction-band threshold state. Following this, calculations of the electroabsorption are carried out, and the theoretical difference spectrum exhibit the same features as in Fig. 13, with a high-energy oscillation beginning at precisely the B_u state identified as the conduction-band threshold state. Details of the wave-function analysis are given below.

We have argued in the case 1 subsection that one of the characteristics of the conduction-band threshold state nB_u is that it has a strong dipole coupling with the mA_g, where the mA_g is identified from its unusually large dipole moment with the $1B_u$. Because of the large value of $U-V$, there still exist ten spin-wave states below the $1B_u$ exciton. The mA_g should therefore still be the $11A_g$. This is confirmed from examining the transition dipole moments $\langle kA_g|\mu|1B_u\rangle$ for all k. The transition dipole moment between the $11A_g$ and the $1B_u$ is 1.9795, which is to be compared with $\langle 1B_u|\mu|1A_g\rangle=0.5567$. All other transition dipole moments between the $1B_u$ and the various A_g states are one to three orders of magnitude smaller. Once the mA_g is identified, the nB_u can be identified as the higher B_u state with a very large dipole moment with the mA_g. This consideration leads to the identification of the $9B_u$ as the nB_u. Because of the very large total number of B_u states, we present only representative data to demonstrate this behavior. In Table IV, we present the transition dipole moments $\langle 11A_g|\mu|kB_u\rangle$ for $k=2-15$. The unique behavior of the $9B_u$ is immediately obvious. We have verified that B_u states above the $15B_u$ have transition dipole moments with the $11A_g$ that are two to three orders of magnitude smaller.

TABLE IV. Transition moments $\langle jB_u|\mu|11A_g\rangle$ ($j>1$) for $N=8$, $U=10$, $V=3$, and $\delta=0.1$. These are to be compared with $\langle 1B_u|\mu|11A_g\rangle=1.9795$. The $1B_u$ is at energy 6.4004. The $11A_g$ is the dominant mA_g state. Note the very large transition dipole moments between the $11A_g$ and the $9B_u$, identifying the latter as the nB_u. B_u states higher than $15B_u$ have small dipole moments with the $11A_g$.

Quantum number j of the B_u states	Energy of jB_u in units of t	$\langle jB_u\|\mu\|11A_g\rangle$
2	7.1575	−0.4841
3	7.3809	−0.3274
4	7.6361	0.2097
5	7.8241	0.0130
6	7.8697	−0.1464
7	8.0253	−0.4388
8	8.1036	−0.2459
9	8.1775	1.9299
10	8.2425	−0.1690
11	8.4271	0.0022
12	8.6212	−0.0003
13	8.6727	−0.1685
14	8.6943	0.0468
15	8.8316	0.0404

It was shown for the strongly correlated case that beginning from the conduction-band threshold state, dipole coupling between energetically neighboring states becomes suddenly very large (see Table II and Fig. 11). The magnitudes of dipole moments between the conduction-band states themselves should be even larger than $|\langle mA_g|\mu|1B_u\rangle|$, which is about the largest dipole coupling among the exciton states. We have examined all possible transition dipole couplings, and find that once again the $9B_u$ exhibits such a threshold behavior. In Table V we list what we believe are the lowest conduction-band states and the dipole moments between them. A pair of excitonic B_u states, the $7B_u$ and the $8B_u$, are also included for comparison. States below the $9B_u$ behave as excitons, with each B_u state having one dipole coupling comparable to $\langle mA_g|\mu|1B_u\rangle$ and all other couplings smaller by two to three orders of magnitude. The B_u states above $9B_u$ that are not listed in Table V behave like excitons. The quantum numbers of the conduction-band states do not increase monotonically until the $25B_u$ is reached. This stems from the overlaps between energy manifolds, as shown schematically in Fig. 14(a). Nevertheless, the very distinct behavior of states higher than $9B_u$ and the thresholdlike behavior of $9B_u$ should be obvious from the dipole moments in Table V. The finite-energy gaps between the lowest conduction-band states are expected to vanish in the infinite chain. The complete results are summarized in Fig. 15, which is to be compared with Fig. 11. We have indicated in the figure that the $9B_u$ is the lowest state for which dipole couplings between neighboring states become larger than all dipole couplings between lower-energy exciton states.

We have also evaluated the density-density correlation

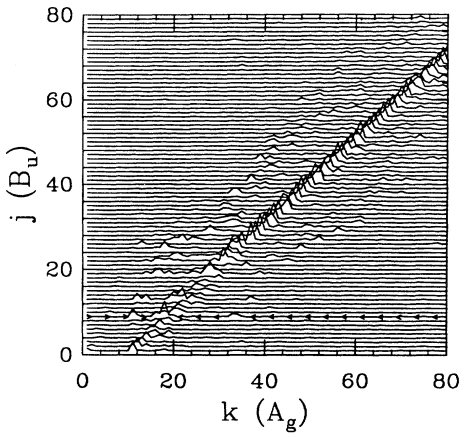

FIG. 15. The three-dimensional plot of the dipole couplings for the parameters of Fig. 14(b). Notice the threshold behavior of $9B_u$, where the dipole couplings between neighboring states become suddenly large. The finite-energy gaps between the lowest conduction-band states will disappear in the infinite chain.

functions $1/N\langle \sum_i (n_i-1)(n_{i+l}-1)\rangle$ to identify the conduction-band threshold state. In Table VI, we have listed these for representative B_u states. They are to be compared with the correlation functions listed in Table IV for the $U=50$, $V=15$ case. Note the sudden change in the correlation function as the $9B_u$ is reached from below, indicating large particle-hole separation. Note that the same B_u states above the $9B_u$ that were classified as excitonic from dipole moment considerations are also the ones that exhibit excitonlike behavior when the correlation functions are examined. Nearly identical behaviors are observed in the case of the $13B_u$ and $19B_u$, both identified as conduction-band states from dipole-moment considerations. On the other hand, the behavior of the B_u states below the $9B_u$ clearly indicate bound particle-hole behavior. Starting from the $25B_u$, we see behavior characteristic of free particle-hole behavior for consecutive B_u states. Exactly analogous behavior is found in the A_g subspace, *viz.* greater particle-hole separation in states identified as conduction-band states from dipole-moment considerations.

We see therefore that three different considerations indicate the same state, *viz.* the $9B_u$ to be the conduction-band threshold state. Small energy gaps exist between conduction-band states themselves in this region until the $25B_u$ is reached. This is a finite-size effect, and we expect these energy gaps to vanish in the infinite-chain limit. Now that the conduction-band threshold state has been identified, we can examine the electroabsorption data. In Fig. 16, we show the linear absorption, which again shows a very sharp exciton, followed by weak transitions to higher B_u states. In Fig. 17(a), we have shown the theoretical $\Delta\alpha$ spectrum, again for $F=0.005$, which shows the same qualitative features as those in Fig. 13(a). Two well-separated signals are shown in the calculated difference spectrum. A redshift of the $1B_u$ exciton is followed by a weak peak caused by the mA_g, and only at even higher energies do oscillatory features stemming from the conduction band begin to appear. Note that the *shape* of the $\Delta\alpha$ in the region $\hbar\omega > 1.2E_g$ is very different from that of the Stark shift of the $1B_u$ exciton. This shape is a characteristic of field-induced splitting of two

TABLE V. Transition dipole moments between conduction-band states beginning from $9B_u$ for $N=8$, $U=10$, $V=3$, and $\delta=0.1$. These numbers are to be compared with $\langle 11A_g|\mu|1B_u\rangle = 1.9795$. The $7B_u$ and the $8B_u$ are included to indicate the thresholdlike behavior of the $9B_u$. Each of these two states below the $9B_u$ behaves exactly like the $1B_u$, with strong dipole coupling to a single excitonic A_g state. The magnitudes of the transition dipole moments between states below $9B_u$ are smaller than $\langle 11A_g|\mu|1B_u\rangle$. The following results should be compared to those presented in Table II.

Quantum number j of B_u states	Quantum number k of A_g states	$E(jB_u)$	$E(kA_g)$	$\langle jB_u\|\mu\|kA_g\rangle$
7	17	8.0253	8.3894	1.3612
8	19	8.1036	8.5962	0.9121
9	16	8.1775	8.3560	1.1012
	18		8.4077	3.6154
13	20	8.6727	8.7479	−1.9211
	21		8.8139	−1.4598
	22		8.8991	−2.7656
	24		9.1262	1.1694
19	17	9.1632	8.3894	1.1258
	27		9.2613	1.4270
	28		9.3757	−2.9535
	29		9.4580	1.2098
22	31	9.6012	9.7363	3.2540
	32		9.7616	−1.0819
	33		9.8818	−0.9696
23	21	9.6438	8.8139	1.0748
	32		9.7616	−2.7803
	33		9.8818	1.9166
	34		9.8990	1.9329
25	18	9.7627	8.4077	1.6588
	33		9.8818	−2.9605
	34		9.8990	2.9931
	48		11.4405	−1.0835

very closely lying states, as would occur within a band. The high-energy feature arising from the conduction band in the $\Delta\alpha$ spectrum in Fig. 13(a) has identical shape. From the absolute energies we can verify that the threshold of the oscillations arises from the $9B_u$ (whose energy is at 1.278 in the unit of the $1B_u$ energy). The signatures in the difference spectrum in this region are much stronger than those in Fig. 13(a), owing to the much smaller V in the present case (a smaller V gives stronger transition dipole matrix elements between the $1A_g$ and the nB_u). The $\Delta\alpha$ for the energy region below E_g is shown as an inset in Fig. 17(a). Notice the absence of any signal from the A_g states that occur below the $1B_u$, even though the vertical scale in the inset is three orders of magnitude smaller. As discussed above, both A_g and B_u states contribute to the oscillation. Similarly to the strong correlated case, we demonstrate this by evaluating the contributions from the A_g and B_u states separately.

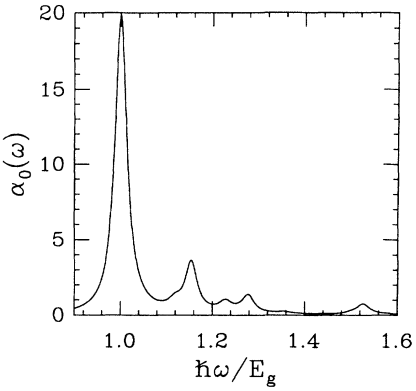

FIG. 16. The calculated linear absorption in arbitrary units, for $N=8$ and the parameters of Fig. 14(b). A half-width of $0.05t$ has been included for calculation of the spectrum. In addition to the absorption to the $1B_u$, weak absorptions occur to the higher B_u excitons.

TABLE VI. Expectation values $1/N\langle \sum_{i=1}^{N-1}(n_i-1)(n_{i+l}-1)\rangle$ as a function of l for $N=8$, $U=10$, $V=3$, and $\delta=0.1$. A large negative value implies a strong particle-hole correlation. The numbers with magnitudes smaller than 0.001 are listed as 0. The excitons are characterized by strong nearest-neighbor correlations, the band states by more delocalized behaviors. Some of the high-energy (above $9B_u$) exciton states exhibit partially delocalized behaviors.

	States			l = 1	2	3	4	5	6	7
Covalent	$1A_g$			−0.044	0.001	−0.001	0	0	0	0
	⋮			⋮	⋮	⋮	⋮	⋮	⋮	⋮
	$10A_g$			−0.003	0	0	0	0	0	0
Band		$1B_u$		−0.115	0.027	−0.032	0.001	−0.008	0	−0.002
		⋮		⋮	⋮	⋮	⋮	⋮	⋮	⋮
		$8B_u$		−0.117	−0.011	−0.014	0	0	0	0
	$9B_u$			−0.068	0.011	−0.010	0.020	−0.030	−0.022	−0.013
		$10B_u$		−0.121	0.008	−0.023	−0.004	−0.002	0	0
		⋮		⋮	⋮	⋮	⋮	⋮	⋮	⋮
		$12B_u$		−0.127	−0.008	0	−0.002	−0.009	0.009	−0.005
	$13B_u$			−0.057	0.007	−0.008	−0.019	−0.031	−0.027	−0.010
		$14B_u$		−0.126	−0.012	−0.005	0.007	−0.004	0	0
		⋮	Exciton	⋮	⋮	⋮	⋮	⋮	⋮	⋮
		$18B_u$		−0.126	−0.005	−0.005	0.002	0.001	0	−0.001
	$19B_u$			−0.049	0.005	−0.010	−0.026	−0.030	−0.020	−0.070
		$20B_u$		−0.119	0.002	−0.006	−0.005	−0.003	−0.003	−0.001
		$21B_u$		−0.120	−0.007	−0.001	−0.001	0	0	0
	$22B_u$			−0.038	0.002	−0.022	−0.042	−0.026	−0.011	−0.003
	$23B_u$			−0.027	0.002	−0.012	−0.030	−0.036	−0.022	−0.006
		$24B_u$		−0.125	0.001	0	−0.001	−0.002	−0.001	0
	$25B_u$			−0.035	−0.002	−0.026	−0.022	−0.011	−0.021	−0.025
	⋮			⋮	⋮	⋮	⋮	⋮	⋮	⋮
	$55B_u$			−0.056	−0.020	−0.018	−0.036	−0.004	−0.10	−0.005
		$55B_u$		−0.141	0.054	−0.043	−0.032	−0.013	−0.002	−0.002
	$56B_u$			−0.057	−0.032	−0.017	−0.021	−0.014	−0.006	−0.011
	⋮			⋮	⋮	⋮	⋮	⋮	⋮	⋮
	$63B_u$			−0.081	0.009	−0.026	−0.023	−0.017	−0.009	−0.010
		$64B_u$	Biexciton	−0.140	0.047	−0.067	0.017	−0.031	−0.005	−0.009
	⋮	⋮		⋮	⋮	⋮	⋮	⋮	⋮	⋮
	$84B_u$			−0.081	0.009	−0.026	−0.023	−0.017	−0.009	−0.010
		$85B_u$		−0.188	0.034	−0.031	−0.022	0.008	−0.013	−0.007
		⋮		⋮	⋮	⋮	⋮	⋮	⋮	⋮

This result is shown in Fig. 17(b). Notice the giant contributions by states of a particular symmetry, as noted already in Fig. 13(b). Once again cancellations occur deep inside the band. The discrete behavior in the oscillations, i.e., the large energy separation between the prominent signals within the conduction band, is the consequence of the finite-size effect. In very long chains, these separations are expected to vanish.

The results for the intermediate Coulomb interaction case can then be summarized as follows. Even though there is considerable overlap between highest-energy exciton states and the lowest-energy conduction-band states, the essential features of the electroabsorption difference spectrum are the same as that in the strongly correlated case. Low-energy A_g states that occur below the $1B_u$ are not observable, the $1B_u$ exciton exhibits a strong Stark shift to the red, and the mA_g exciton occurs as a peak close to the $1B_u$ signal, while at even higher energy there exists an oscillatory structure originating from the conduction band. The shapes of the oscillatory features are the same as those in Fig. 13(a).

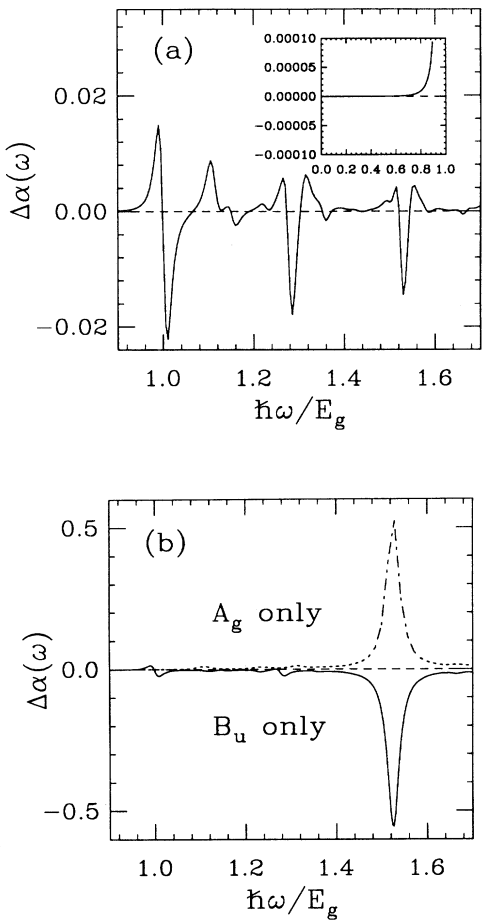

FIG. 17. (a) The calculated electroabsorption difference spectrum, in arbitrary units, for the parameters of Fig. 14(b). The inset shows the electroabsorption in the region below the energy of the $1B_u$ exciton. Notice that the vertical scale here is three orders of magnitude smaller, but no electroabsorption due to the ten A_g states below the $1B_u$ is observed. Notice also the shapes of the high-energy features, characteristic of the energy splitting of proximate levels within the conduction band, as also seen in the high-energy feature in Fig. 13. (b) The individual contributions by the A_g and B_u states to the electroabsorption for the parameters of (a). The units are the same as in (a). Notice that the vertical scale in (b) is an order of magnitude larger than that in (a).

Case 3: Weak-correlation limit, $U=4.0, V=1.5$

This is close to the realistic correlation regime for conjugated polymers. It is futile to calculate the electroabsorption here, as the calculated difference spectrum cannot exhibit the behavior expected in the infinite chain. All intraband gaps are very large for weak interactions in short chains, and finite-size effects dominate linear absorption as well as optical nonlinearity.[48(a)] This is why we have argued elsewhere[41] that the infinite-chain behavior is better represented by calculations involving stronger Coulomb interactions, as in this case the $N\rightarrow\infty$ convergence is faster. Note that the same is true even for the short noninteracting Hückel chains, the dominance of the large intraband gaps can be eliminated only by incorporating an artificially large bond-alternation parameter.[48(b)] For moderate bond alternation, the calculated electroabsorption of a short noninteracting chain is entirely different from the long-chain behavior shown in Fig. 8(b). With a V of only 1.5, the gap between the lowest exciton and the lowest conduction-band state becomes comparable to the gaps within the conduction-band states for short chains, and it becomes impossible to get well-separated signatures in the difference spectrum of finite chains. Our motivation here is then not to compare with experiments (which we believe are better explained by the intermediate correlations calculations), but rather to demonstrate that the qualitative features associated with the conduction-band edge in the intermediate to strong Coulomb interactions can also be observed for the weak-correlated case.

The mA_g in the present case is found in the usual manner, by evaluating dipole moments between the $1B_u$ and all excited A_g states. Such a calculation indicates the $6A_g$ to be the mA_g, with $|\langle 6A_g|\mu|1B_u\rangle|$ being 2.7127, larger than all other excited A_g-1B_u couplings by one to three orders of magnitude. For comparison, $|\langle 1A_g|\mu|1B_u\rangle|$ is 1.2949, smaller by a factor of 2. One of the ways we found the nB_u in the previous cases was to determine the still higher unique B_u whose transition dipole moments with the mA_g were almost equally large. In the present case, this approach identifies the $4B_u$ as the nB_u; the dipole moment $|\langle 6A_g|\mu|4B_u\rangle|=2.2464$ is clearly large. It is known from the above that the nB_u is the lowest B_u with very large dipole moments with neighboring *higher-energy-band* A_g states (see Tables II and V). We found that the $4B_u$ satisfies this criterion since the dipole moments $|\langle 4B_u|\mu|12A_g\rangle|$, $|\langle 4B_u|\mu|13A_g\rangle|$, and $|\langle 4B_u|\mu|15A_g\rangle|$ are 2.0478, 2.3590, and 1.0474, respectively, while states $1B_u$, $2B_u$, and $3B_u$ do not possess these characteristics. The third approach by which we

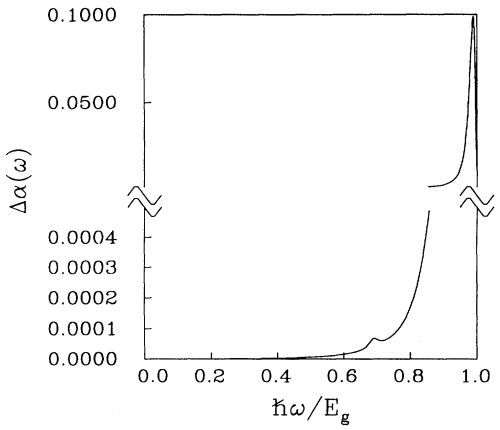

FIG. 18. The calculated electroabsorption difference spectrum, in arbitrary units, for $N=8$, $U=4$, $V=1.5$ $t=1$, and $\delta=0.1$ in the energy region below the $1B_u$ exciton. Note the absence of electroabsorption due to the A_g states in this region.

identified n was by examining the density-density correlation functions (see Tables III and VI). In the present case, because of the strong overlaps between states, it is difficult to classify the various states by examining individual correlation functions. Instead, we chose to measure the *average* particle-hole separation for the lowest B_u states. This value is close to 1.5 lattice constants for the first three B_u states, but jumps to 3 for the $4B_u$. This separation is to be compared to mean particle-hole separations of 3.9 lattice constants and 3.29 lattice constants for the nB_u in the two previous cases, $U=50$, $V=15$ and $U=10$, $V=3$, respectively. The average particle-hole separations in the nB_u are therefore quite close for the three cases. Thus from three different considerations we are again able to identify the same B_u state as the conduction-band threshold state. We believe that this strongly indicates a universality within the one-dimensional extended Hubbard models, and in the infinite-chain limit, where the discreteness between the band states has disappeared and that the electroabsorption corresponding to even these moderately weak Coulomb interactions would resemble that for $U=10$, $V=3$.

While we do not show the calculated electroabsorption for energies above E_g for such small parameters, the energy region *below* E_g is still significant. This is because in the energy region above E_g it is not possible to simulate the closely spaced conduction-band levels from finite-chain calculations for weak interactions. On the other hand, states below E_g are known to be discrete even at infinite N, and the calculated electroabsorption spectrum here is relevant. In Fig. 18, we show the calculated electroabsorption below E_g for $F=0.005$. Notice again the absence of any significant feature due to two-photon states here (the vertical scale in the low-frequency region of the $\Delta\alpha$ spectrum is three orders of magnitude smaller than the $\Delta\alpha$ due to the $1B_u$ exciton).

IV. THE nB_u AS AN ESSENTIAL STATE IN THG AND TPA

Although we have focused on electroabsorption and the information it provides about the underlying electronic structure of isolated linear conjugated strands, the mechanism of electroabsorption discussed here has strong implications about other third-order optical nonlinear processes such as THG and TPA.[30] This is to be expected, as electroabsorption is but one special case of the general third-order nonlinearity. Since THG gives information on both one- and two-photon states, we focus on the susceptibility relevant for THG. The numerator of the susceptibility that describes TPA is the same as the THG susceptibility, so that the same essential states describe TPA, while two-photon absorptions to the nonessential even-parity states should have very weak intensities in the infinite-chain limit. The formal expression for the susceptibility relevant to THG is given by

$$\chi^{(3)}(-3\omega;\omega,\omega,\omega)=\sum_{j,k,l}\langle 1A_g|\mu|jB_u\rangle\langle jB_u|\mu|kA_g\rangle\langle kA_g|\mu|lB_u\rangle\langle lB_u|\mu|1A_g\rangle \times\{D_1(\omega)+D_1(-\omega)+D_2(\omega)+D_2(-\omega)\}\ , \tag{7a}$$

where

$$D_1^{-1}(\omega)=(\omega_{jB}+3\omega)(\omega_{kA}+2\omega)(\omega_{lB}+\omega)\ , \tag{7b}$$

$$D_2^{-1}(\omega)=(\omega_{jB}+\omega)(\omega_{kA}+2\omega)(\omega_{lB}-\omega)\ . \tag{7c}$$

The triple sum in Eq. (7a) is over all possible A_g and B_u states, and all the energies are with respect to the ground-state energy. Earlier works[19–22] have emphasized the very strong role played by the mA_g in $\chi^{(3)}$ processes because of the giant dipole coupling between the mA_g and the $1B_u$. The mA_g in its turn is very strongly coupled to the nB_u, as shown in Sec. III, implying that the nB_u is also involved strongly in $\chi^{(3)}$ processes. In the following, we give the detailed mechanism of $\chi^{(3)}(-3\omega;\omega,\omega,\omega)$.

From the above expression for $\chi^{(3)}$, three-photon resonances at energies that are one-third the energies of dominant B_u states, and two-photon resonances at energies that are half the energies of the dominant two-photon states, are expected. The occurrence of only a few resonances in the THG of π-conjugated polymers, in spite of practically an infinite number of states in the infinite chain, is a clear signature of the existence of a few dominant states (hereafter, "essential states") that determine the bulk of the nonlinearity. Theoretical work on $\chi^{(3)}$ has

largely focused on *trans*-polyacetylene, both because this has been historically considered the prototype conjugated polymer and because this was the first system for which the THG spectrum was obtained over a wide frequency range.[11] The THG spectrum of *trans*-polyacetylene exhibits a strong three-photon resonance at one-third the optical gap, and a weaker resonance at nearly half this gap. The latter has been commonly attributed to be a two-photon resonance, and the bulk of theoretical activity has focused on finding an A_g state that is nearly degenerate with the optical state (such that the two-photon resonance can occur at midgap), and that has a strong dipole coupling with the $1B_u$ (in order that this can be one of the dominant states). There exist several theoretical papers,[19–22,38,39] including our own, which discuss this aspect of the THG spectrum, and although they differ in details, the essential implications are similar. Based on such considerations, for example, Dixit, Guo, and Mazumdar have recently formulated a three-level "essential states" picture of optical nonlinearity that includes the ground state, the optical state, and the mA_g state.[21] However, this picture is not complete. Our later work[30] has indicated that there exist four, and not three, essential states, the fourth being the nB_u.

As with the electroabsorption, we begin the theory of THG with the noninteracting model, which clearly indicates the necessity of having four essential states. The discussion in Sec. III A emphasized the need to consider two B_u states for each A_g contributions to the $\chi^{(3)}$. We consider the $2A_g$ in Fig. 7 as an example. From our discussion in Sec. III A,

$$\langle 1A_g|\mu|1B_u\rangle\langle 1B_u|\mu|2A_g\rangle = -\langle 2A_g|\mu|2B_u\rangle\langle 2B_u|\mu|1A_g\rangle , \quad (8)$$

in the infinite-chain limit. $\chi^{(3)}$ processes involving the $2A_g$ can therefore be classified into "direct" terms:

$$1A_g \rightarrow 1B_u \rightarrow 2A_g \rightarrow 1B_u \rightarrow 1A_g , \quad (9a)$$

$$1A_g \rightarrow 2B_u \rightarrow 2A_g \rightarrow 2B_u \rightarrow 1A_g , \quad (9b)$$

in which the same B_u state occurs twice, and "cross" terms

$$1A_g \rightarrow 1B_u \rightarrow 2A_g \rightarrow 2B_u \rightarrow 1A_g , \quad (10a)$$

$$1A_g \rightarrow 2B_u \rightarrow 2A_g \rightarrow 1B_u \rightarrow 1A_g , \quad (10b)$$

in which different B_u states appear. Each arrow in the above expressions represents a dipole-allowed interband or intraband transition, and therefore corresponds to a matrix element in Eq. (7a). From Eq. (8), the products of the matrix elements in the cross terms are negative, while the products are necessarily positive in the direct terms. In the infinite-chain limit the energies of the $1B_u$ and the $2B_u$ converge to the same value, and the direct and cross terms cancel. Thus the net $\chi^{(3)}$ contribution from the band-edge A_g states vanishes in the infinite-chain limit, and, therefore, there is no two-photon resonance in the midgap region within the rigid-lattice noninteracting model.[38–42] This result implies that (a) the inclusion of electron correlations is essential for the explanation of the THG spectrum of the real materials, and (b) there exist four, rather than three, essential states.

Our earlier results[21,22] and the results in Sec. III indicate that within interacting electron models the mA_g plays the same role as the $2A_g$ in the noninteracting model, in having a giant transition dipole moment with the $1B_u$. Similarly, the nB_u plays the same role as that of the $2B_u$, because of its very large coupling with the mA_g. Furthermore, due to nonzero Coulomb interactions, the oscillator strength of the linear absorption is very strongly concentrated in the $1B_u$, and any essential-state picture is even more valid. As in the case of the noninteracting electron model, $\chi^{(3)}$ channels in the interacting electron model involving an arbitrary A_g state are also of two different kinds: (i) those which involve the same B_u state twice; and (ii) those in which two different B_u states occur. Direct evaluations of dipole moments indicate these two different types of processes still to have opposite signs, such that the symmetry relationships of the noninteracting model carry over to the interacting case. Then the most relevant $\chi^{(3)}$ channels involving the mA_g are

$$1A_g \rightarrow 1B_u \rightarrow mA_g \rightarrow 1B_u \rightarrow 1A_g , \quad (11a)$$

$$1A_g \rightarrow nB_u \rightarrow mA_g \rightarrow nB_u \rightarrow 1A_g , \quad (11b)$$

with the $1B_u$ and the nB_u occurring twice, and

$$1A_g \rightarrow 1B_u \rightarrow mA_g \rightarrow nB_u \rightarrow 1A_g , \quad (12a)$$

$$1A_g \rightarrow nB_u \rightarrow mA_g \rightarrow 1B_u \rightarrow 1A_g , \quad (12b)$$

with two different B_u states. Because of the opposite signs of the two kinds of terms in the expansion for $\chi^{(3)}$, the strength of the two-photon resonance due to the mA_g is reduced considerably. For a simple Hubbard model ($V=0$) in which there is no exciton binding, nB_u is still a low-level-band B_u state ($n=2$ or 3 in short chains) that approaches the $1B_u$ at the infinite-chain limit, and the two-photon resonance vanishes again.[42] For nonzero V, the path in Eq. (11b) contributes only weakly to $\chi^{(3)}$, owing to the smaller value of $|\langle 1A_g|\mu|nB_u\rangle|$, but contributions from paths in Eqs. (12a) and (12b), with three out of four of the couplings large, are non-negligible. Therefore, the dominant $\chi^{(3)}$ channels are the ones given by Eqs. (11a), (12a), and (12b), which are shown in Figs. 19(b) and 19(c). In addition to these channels, a process involving only the $1A_g$ and $1B_u$ [see Fig. 19(a)] can also strongly contribute to $\chi^{(3)}$. There is a finite-energy gap between the $1B_u$ and the nB_u for $V\neq 0$, and $|\langle 1A_g|\mu|1B_u\rangle|$ and $|\langle 1A_g|\mu|nB_u\rangle|$ are, in this case, unequal even in the infinite-chain limit. Thus a nonvanishing intensity of the two-photon resonance due to the mA_g is expected.[42] We have previously[21,22] argued that, in the ideal infinite chain, the mA_g occurs energetically very close to the $1B_u$, and this should give a two-photon resonance very close to half the optical gap.

Apart from a nonvanishing intensity of the two-photon resonance, the interacting model also predicts a second three-photon resonance[30(b)] due to the nB_u. This is be-

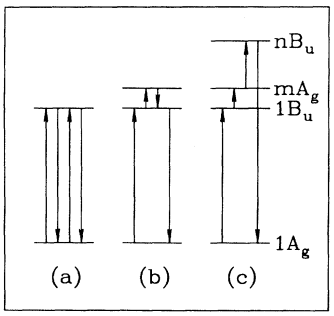

FIG. 19. The three dominant channels for $\chi^{(3)}$ involving the $1A_g$, $1B_u$, mA_g, and nB_u states. The contributions to $\chi^{(3)}$ by (b) and (c) are of opposite signs at all frequencies.

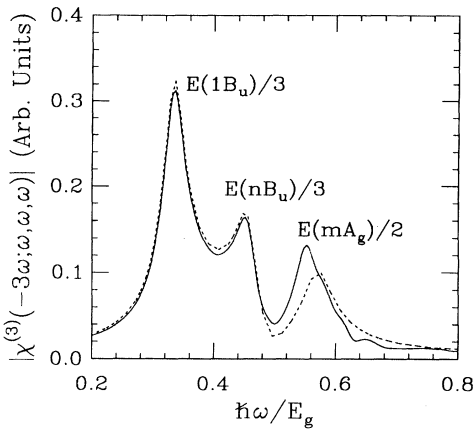

FIG. 20. The THG spectrum for $N=8$, $U=10$, $V=3.5$, $t=1$, and $\delta=0.1$. Solid line, the THG spectrum obtained by summing over all states; dashed line, the spectrum obtained by summing over only the essential states. In the infinite chain, such a three-peak spectrum is expected even for smaller Coulomb interactions, as long as the Coulomb interactions are large enough to give exciton binding.

cause in paths (12a) and (12b), three out of four of the steps involve very strong couplings, unlike that for any nonessential states, for which two or more of the couplings are considerably weaker. Therefore, like the mA_g, the nB_u is also unique.

Exact numerical calculations have been performed to confirm this interpretation. As discussed in Sec. III, it is difficult to reproduce in short chains the features associated with the continuum with realistic Coulomb interactions. Furthermore, additional finite-size effects such as double resonances[48(a)] dominate $\chi^{(3)}$ calculations in short chains with realistic Coulomb interactions. Such double resonances occur whenever zeros are simultaneously approached by at least two terms in the parentheses constituting the same denominators in Eq. (7), which is a common occurrence in finite chains with discrete spectra.[48] Therefore we report our result for the calculations for moderately large parameters $U=10$, $V=3.5$. A slightly larger V than for the electroabsorption case was chosen merely to increase the separation between the three-photon resonances due to the $1B_u$ and the nB_u. In Fig. 20, we show the results of our exact numerical calculation. The peak at the lowest energy corresponds to the usual three-photon resonance due to the $1B_u$, the second peak is a three-photon resonance due to the nB_u, and the third corresponds to a two-photon resonance due to the mA_g. Our earlier numerical calculations involved only three states (the $1A_g$, $1B_u$, and mA_g) and therefore missed the very important role of the nB_u. The solid curve in Fig. 20 is based on a calculation that includes the *complete* energy space. The dashed curve corresponds to a calculation that retained only the four essential states. Notice that the essential-state calculation is able to reproduce quantitatively the THG spectrum obtained when all 485 A_g states and 460 B_u states are retained. We shall argue in the next section that the three-photon resonance due to the nB_u has been observed in THG experiments in the past, but has often been misidentified[10,12,17,20] as a two-photon resonance due to the $2A_g$. We discuss below (and, in greater detail, in Appendix B) why the nonessential states such as the $2A_g$ contribute weakly to $\chi^{(3)}$ processes (as in electroabsorption) in the infinite-chain limit, even within interacting models. Resonances resulting from such states therefore would have extremely weak (perhaps vanishing) intensities.

Nonessential A_g states have two characteristics. First, they have weak dipole couplings[21,22] with the $1B_u$. Second, and even more important, they continue to be equally strongly dipole coupled to two B_u states whose energies approach each other in the infinite-chain limit (note that this is not true for the essential mA_g state; the characters and the energies of the $1B_u$ and the nB_u are different). Thus their dipole moments with these two B_u states are nearly the same in the infinite-chain limit, and, due to the cancellation between the direct and the cross terms involving this A_g state and the two B_u states, the intensity of the two-photon resonance is vanishingly weak. This effect and the nonparticipation by nonessential states such as the $2A_g$ in the electroabsorption are therefore related. A more quantitative discussion is presented in Appendix B, where we show that even for realistic Coulomb interactions the intensity of the $2A_g$ resonance is weak.

Summarizing this section, four essential states are necessary to describe the dominant channels for third-order optical nonlinearity. These are the $1A_g$, $1B_u$, mA_g, and nB_u. Nonzero Coulomb interactions lead to a concentration of the oscillator strength of the linear absorption in the $1B_u$ exciton, as a result of which the four essential states can reproduce quantitatively the nonlinearities calculated for the entire energy spectrum. Three different resonances are expected in the THG, two three-photon resonances due to the $1B_u$ and nB_u, and a two-photon resonance due to the mA_g. Excitonic behavior is essential for a two-photon resonance with nonvanishing intensity in the frequency region (<1.2 eV) of experimental interest. Thus both on-site and intersite Coulomb interactions are necessary for a complete description of optical nonlinearity.

V. COMPARISON OF THEORY WITH EXPERIMENTS

In this section, we make comparisons between experiments and theory. We will discuss both electroabsorption as well as a few representative THG and TPA spectra. The experimental electroabsorption spectrum shows an oscillatory signal in addition to the Stark shift of the exciton at an energy of 2.35 eV. The theoretical calculations, done in several steps, indicate that such an oscillatory signal originates from the conduction band. Within the theory, excitonic B_u states exhibit simple shifts, while excitonic A_g states lead to peaks in the difference spectrum. The oscillation originates from the participation of proximate A_g and B_u states which are very close in energy. The contributions to $\Delta\alpha$ by A_g and B_u states in the conduction band are very large, and cancel for states inside the conduction band. This is to be expected within the mechanism of electroabsorption postulated here. While the details are different, the mechanism of the electroabsorption does have similarities to that for conventional inorganic semiconductors.[46] It is not a coincidence that the energy of the high-energy signals in electroabsorption and the photoconductivity thresholds[43] in DCH and other polydiacetylenes are the same.

In the presence of Coulomb correlations, a prominent peak originating from the mA_g is anticipated (see Figs. 13 and 17). From both our earlier work[21,22,41,47] and the present work, we anticipate that the mA_g in the linear-chain polymers is very close in energy to the $1B_u$. In the experimental $\Delta\alpha$ spectrum, a large positive contribution is present on the high-energy side of the Stark shift of the exciton below the energy of the lowest vibronic sideband (see Fig. 2). It is conceivable that this feature has contributions from the energy shift of the vibrational sideband seen in the linear absorption spectrum. However, the positive part of $\Delta\alpha$ here is much larger than the negative part, which is not expected for a simple shift. It is therefore possible that this part of the electroabsorption spectrum has contributions from both the mA_g and the vibrational sideband. In order to probe this further, we have compared the actual $\Delta\alpha$ spectrum with the derivative spectrum of the experimental linear absorption (see Fig. 4). Any feature that survives subtraction of these two spectra is a new field-induced feature. Such a feature is seen in Fig. 4 near 2.0 eV, suggesting participation by the mA_g. Similar positive contributions on the high-energy side of the exciton have been observed by Jeglinski and Vardeny in a number of π-conjugated polymers.[49] Further work is necessary to determine the role of the mA_g in electroabsorption.

In contrast to the mA_g, any signature related to the $2A_g$ is missing both in the experimental difference spectrum as well as in the theoretical calculations. The reason for this has already been given in Sec. III. A more quantitative treatment is given in Appendix B. Indeed, among all the electroabsorption experiments performed in the PDA's, we have come across only one work[50] that finds an electroabsorption signal at 1.75 eV in PTS-PDA (PTS stands for paratoluenesulphonate), below the exciton. The occurrence of photoconductivity at the same energy threshold suggests that this is the signature of a charged impurity, and not due to the $2A_g$ (Ref. 50). Other evidence linking this low-energy feature in electroabsorption to impurity effects can be found in the original reference. The assignment of this signal to the $2A_g$ is from energy considerations alone,[20] and, as is shown here, intensity considerations preclude this assignment.

One other important conclusion regarding A_g states is as follows. Based on very similar numerical calculations but a quite different $N\rightarrow\infty$ extrapolation, it has been argued[20] that the mA_g in PDA's occurs at very high energy, $\sim 1.5\times E(1B_u)$, which would place it *above* the conduction-band threshold. Elsewhere we have discussed why the particular extrapolation technique employed by the authors of Ref. 20 may not be appropriate.[22] We have performed our calculations for a very wide range of parameters, including small Coulomb interactions, and have determined the conduction-band threshold in each case. In all cases, we have found that the mA_g necessarily occurs below the conduction-band threshold. This would also agree with a physical interpretation of third-order optical processes that has been presented by us.[41] Note further that since the conduction band is composed of numerous closely spaced A_g and B_u levels, there is no logic for a unique conduction-band A_g state to be the dominant two-photon state. Any such unique state should therefore necessarily be excitonic. Thus while we are unable to calculate the exact energy of the mA_g in the infinite chain, we are able to put an absolute upper bound, the conduction-band threshold, to its energy. The prediction regarding the close proximity of the mA_g to the $1B_u$ is supported by the elaborate experiments by van Beek, Kajzar, and Albrecht,[14] who place the $1B_u$ at 21 250 cm^{-1} and the mA_g at 22 200 cm^{-1}, respectively, in β carotene.

We now compare theoretical predictions and experimental THG spectra. Our work predicts two three-photon resonances, with the intensities of both being larger than the two-photon resonance due to the mA_g. In many PDA's, THG measurements show two resonances.[9,10,12,13] Of these, the low-energy one is easily assigned to the three-photon resonance due to the exciton, from the comparison with the linear absorption spectrum. The second peak (or maximum) in the THG spectra on the high-energy side is *below* the exact midgap. This second resonance has therefore commonly been assigned[9,10,12,20] to a two-photon resonance due to the $2A_g$, which occurs below the $1B_u$. Notice that *only* the argument for assigning this high-frequency resonance to a two-photon resonance is based on the absence of linear absorption at three times the resonance frequency. However, the strong binding energy of the exciton in the PDA's precludes observable linear absorption to the conduction-band threshold (the nB_u), which, as we have shown in this work, participates strongly in nonlinear optical processes. We therefore strongly believe that the higher-frequency resonance in the PDA's is not a two-photon resonance at all, but a three-photon resonance due to the nB_u. We believe that the three-photon resonance due to the nB_u has also been seen in the THG of a

blue form of PDA by Hasegawa *et al.*, who performed electroabsorption on the same material.[22] The electroabsorption shows the high-energy signal originating from the conduction band, while, in their THG spectrum, there exists a resonance at one-third the energy of the conduction-band threshold. The energy region where the mA_g resonance is predicted to occur has not been probed.

Our assignment is supported most strongly from intensity considerations. The high-frequency resonance in PDA's occasionally has a relatively strong intensity, the strength sometimes being nearly our-third to one-half of the three-photon resonance[10,12] due to the $1B_u$. Although from energy considerations alone[20] the assignment of the origin of this resonance to the $2A_g$ seems plausible, the argument on the intensity of such a resonance (see Sec. IV and Appendix B) makes this a highly improbable scenario. Our calculations indicate that the intensity of the two-photon resonance due to the $2A_g$ is very small as a result of cancellation effect of the kind discussed in this paper. Since the cancellation becomes stronger as the chain length increases, *the relative intensity of the $2A_g$ resonance in finite chains corresponds to an upper limit for PDA's.* In spite of this, we have never been able to find an intensity of the two-photon resonance due to the $2A_g$ anywhere near the observed intensity: the calculated relative intensities are invariably very small. This is in close agreement with the experimental result of van Beek, Kajzar, and Albrecht.[14]

We point out that energy considerations also lead us to the same conclusion. Perhaps the clearest demonstration that the second resonance in the THG of PDA's is not a two-photon resonance due to the $2A_g$ is obtained by examining the data on a material for which both direct two-photon absorption (TPA) and THG have been done,[9,12,41] poly-4BCMU PDA (poly[5,7-dodecadiyne-1,12diol bis(*n*-butoxycarbonylmethylurethane)]). A weak hump at 1140 nm in the TPA spectrum of poly-4BCMU is assigned to the $2A_g$ (the very weak intensity of this resonance is in agreement with our discussion of the cancellation that reduces the TPA as well as the THG resonance intensity). In the THG spectrum, the resonance at the higher-energy side of the $1B_u$ three-photon resonance occurs at 1350 nm. This is contradictory to the TPA result if this peak is attributed to the $2A_g$. Thus even from energy considerations this second resonance cannot be linked to the $2A_g$. Based on the theory and all of the above experimental results, we believe that the occurrence of two three-photon resonances in isolated strands is the norm rather than the exception.

Two three-photon resonances have recently been predicted by Abe *et al.*,[51] who also assign the second THG resonance in PDA's to the three-photon resonance due to the conduction-band threshold. In agreement with the present work (see also Ref. 30), they also find the dominant mA_g bounded by the exciton and the conduction-band threshold. However, they place the mA_g exciton very close to the conduction band, in contrast to our prediction of its lying closer to the $1B_u$. The method used by Abe *et al.*[51] is finite-order configuration interaction, retaining only single excitations (single-CI), and fails to find the A_g states below the $1B_u$. Furthermore, within the single-CI approach, the energy of the conduction-band threshold is independent of U, while the correct result is that this energy increases monotonically with U. Thus we agree with these authors on the assignment of the THG resonances and the placement of the mA_g below the conduction-band threshold, but we believe that the relatively high energy of the mA_g predicted by them is an artifact of the single-CI approach.

In comparing theoretical predictions with experiments, we have so far limited our discussions to the PDA's. As far as the entire class of π-conjugated polymers are concerned, two opposing viewpoints exist in the literature. It has been claimed that the bulk of the π-conjugated polymers can be described within a modified SSH model with weak electron-electron interactions, and only in the PDA's are the interactions strong, which therefore form a class by themselves.[52] Within this picture electron-phonon interactions play a major role in systems other than the PDA's, and the nonlinear optical properties of a system such as *trans*-polyacetylene is predominantly determined by the degenerate nature of its ground state and the generation of virtual soliton-antisoliton pair.[53] The very large nonlinearity of *trans*-polyacetylene, as compared to that of *cis*-polyacetylene,[54] supports this viewpoint. An alternate viewpoint is that the optical gaps in all π-conjugated polymers are dominated by Coulomb interactions, with electron-phonon interactions and confinement interactions playing a subsidiary role.[33] A large number of anomalous observations (e.g., the occurrence of the $2A_g$ below the $1B_u$ in finite oligomers of both *trans*-polyacetylene and polydiacetylenes[36]) have been explained consistently within this approach. This is the model applied here to the PDA's, and a rigid-lattice picture[19–22,38–42,51] is assumed. Within our model the principal differences between the PDA's and other conjugated polymers are the negligible interchain interactions (Coulomb and interchain hopping) in the PDA's due to large sidegroups as well as a large exciton binding energy due to a very short triple bond (note that a short bond not only implies a large hopping integral, but also a large intersite Coulomb interaction). Recent work has suggested exciton polarons in systems such as polyphenylenevinylene (PPV).[55] Thus there seems to be experimental evidence for both classes of theoretical models, suggesting that a proper theoretical model should be able to treat both electron-phonon and electron-electron interactions on an equal basis. Theoretical work on interchain interactions with Coulomb correlated Hamiltonians would also be necessary. We believe that in principle it should also be possible to explain the broad features of the nonlinear optical properties of the polyacetylenes within our rigid-band essential-state model. The occurrence of the mA_g very close to the $1B_u$, as well as the weak role played by the $2A_g$ in β carotene,[14] a finite oligomer of *trans*-polyacetylene, partially supports this viewpoint. In the case of *trans*-polyacetylene, THG measurements have been carried out over a broad frequency range, but nevertheless only two resonances are seen,[11] in

contrast to the three predicted here. Within the present model, this could be due to a strong overlap of states arising from interchain interactions. Assuming that the nB_u occurs at an energy close to that in the PDA's, a three-photon resonance is expected at about 0.8 eV, while the two-photon resonance is predicted at 0.9–1.0 eV.[21] Further work is required to clarify the situation in polyacetylene. Finally, although theoretical analysis of polysilanes requires modifications, initial analysis[34] suggests that THG should once again find three resonances. This has recently been confirmed experimentally.[56] We believe that it is significant that the relative intensities of the three resonances are qualitatively similar to that predicted in Fig. 20, *viz.* the intensities of the resonances decrease with increasing frequency.

ACKNOWLEDGMENTS

The authors would like to acknowledge support from NSF (Grant No. ECS-89-11960) and the AFOSR (Grant No. F49620-93-1-0199). Work by S.N.D. was performed under the auspices of the U.S. Department of Energy for the Lawrence Livermore National Laboratory under Contract No. W-7405-Eng-48.

APPENDIX A: THE VALENCE BOND PICTURE FOR WAVE FUNCTIONS

The excitonic states, the conduction band, and the biexciton states are all described within the total-energy picture in the present paper. Because of the unconventional nature of this description, we give detailed valence bond descriptions of the various wave functions. Since our purpose is illustration, we only demonstrate the case of $N=4$, for which the total number of valence bond basis functions is manageable.

The valence bond diagrams are obtained in the usual manner, by constructing many-electron basis functions with sites having all possible electron occupancies, and then constructing singlet bonds between singly occupied sites. Our notation will be as follows. A doubly occupied site will be represented by a cross ($\times$), an empty site by a dot ($\cdot$), and singlet coupled singly occupied sites by a bond joining these. VB diagrams in which any two bonds cross are not linearly independent and can be rewritten as linear combinations of diagrams with noncrossing bonds.[57]

For $N=4$ there are 20 linearly independent VB diagrams. The A_g subspace consists of linear combinations that are symmetric with respect to the mirror-plane symmetry as well as the electron-hole symmetry.[58] The electron-hole symmetry interchanges a double occupancy and an empty site. The B_u subspace consists of linear combinations that are unsymmetric with respect to both these symmetries. The two different sets with different symmetries for $N=4$ are shown in Fig. 21, where there are nine A_g functions and six B_u functions. These 15 linear combinations of the 20 basic diagrams describe all linear and nonlinear optical processes.

The VB functions in Fig. 21 can be further classified according to the number of double occupancies. Functions with zero double occupancies are referred to as covalent. The B_u states are therefore necessarily ionic, i.e., they contain at least one double occupancy. Finite t mixes all functions within a given subspace, but for nonzero U (in particular moderately large U) the ground state is heavily weighted by the covalent functions. This implies that the optical states are the B_u states heavily dominated by singly ionic functions with one double occupancy. If V is also nonzero, these singly ionic states can be further classified into those in which the $\times$ and the $\cdot$ occur as nearest neighbors, and those in which they are separated. The former are the excitons, while the latter constitute the conduction band. Note that A_g states can also be excitonic or bandlike, although they are not dipole coupled to the ground state. This basic description remains valid for $U, V > |t|$ even if finite t mixes the various valence bond functions.

A_g Basis	B_u Basis
$\|1+\rangle =$ — —	
$\|2+\rangle =$ ⌜—⌝	
$\|3+\rangle = (\times\cdot\,—)+(—\,\cdot\,\times)+(\cdot\times—)+(—\,\times\,\cdot)$	$\|1-\rangle = (\times\cdot\,—)+(—\,\cdot\,\times)-(\cdot\times—)-(—\,\times\,\cdot)$
$\|4+\rangle = (⌜\times\cdot⌝)+(⌜\cdot\times⌝)$	$\|2-\rangle = (⌜\times\cdot⌝)-(⌜\cdot\times⌝)$
$\|5+\rangle = (⌜\times⌝\,\cdot)+(\cdot\,⌜\times⌝)-(⌜\cdot⌝\times)-(\times⌜\cdot⌝)$	$\|3-\rangle = (⌜\times⌝\,\cdot)-(\cdot\,⌜\times⌝)+(⌜\cdot⌝\times)-(\times⌜\cdot⌝)$
$\|6+\rangle = (\times—\,\cdot)+(\cdot\,—\times)$	$\|4-\rangle = (\times—\,\cdot)-(\cdot\,—\times)$
$\|7+\rangle = (\times\cdot\times\cdot)+(\cdot\times\cdot\times)$	$\|5-\rangle = (\times\cdot\times\cdot)-(\cdot\times\cdot\times)$
$\|8+\rangle = (\times\cdot\cdot\times)+(\cdot\times\times\cdot)$	
$\|9+\rangle = (\times\times\cdot\,\cdot)+(\cdot\,\cdot\times\times)$	$\|6-\rangle = (\times\times\cdot\,\cdot)-(\cdot\,\cdot\times\times)$

FIG. 21. Valence-band basis functions within the A_g and B_u subspaces for $N=4$. Here crosses ($\times$) and dots ($\cdot$) are double occupancies and empty sites, respectively, and a bond implies singlet coupling [e.g., $|2+\rangle = (c^+_{1,\uparrow}c^+_{4,\downarrow} - c^+_{1,\downarrow}c^+_{4,\uparrow})(c^+_{2,\uparrow}c^+_{3,\downarrow} - c^+_{2,\downarrow}c^+_{3,\uparrow})|0\rangle$].

Referring to Fig. 21, we see that there are two VB basis functions ($|3+\rangle$ and $|4+\rangle$) in the A_g subspace, and two ($|1-\rangle$ and $|2-\rangle$) in the B_u subspace that are singly ionic with a double occupancy and an empty site as nearest neighbor. Therefore for large enough U and V, in the $N=4$ case the lowest two B_u states are excitonic, while the third and the fourth A_g states have the same character (the lowest two A_g are the ground state, and a covalent excitation). The quantum number n of the B_u state that forms the conduction-band threshold in this simple case of $N=4$ with nearest-neighbor intersite interaction is 3. Since there are only two B_u basis functions ($|3-\rangle$ and $|4-\rangle$ in Fig. 21) which are singly ionic with the particle and the hole separated by more than one lattice constant, there can be only two conduction-band states of B_u symmetry. For the same reason there are only two conduction-band-like states of A_g symmetry. At still higher energy we expect two biexcitons, one of A_g and one of B_u symmetry, defined to be states dominated by doubly ionic valence bond functions with per-

fectly alternating double occupancies and empty sites. This description is altered only quantitatively for moderate U and V, where, due to greater mixing between VB functions, the conduction band can start from a B_u state with quantum number n less than its saturation value of 3.

As we go to longer and longer chains, the same description persists. The only differences are as follows. First, the number of singly ionic valence bond functions with nearest-neighbor double occupancy and empty sites increases with N, and all these give exciton states. Thus the value of n, the quantum number of the B_u state at the conduction-band threshold, increases with size. However, this increase occurs in a predictable manner, such that from symmetry considerations of VB functions alone it is easy to predict the saturation values of n for a given N. Second, and more important, the exciton states within the nearest-neighbor interaction model are only those with nearest-neighbor double occupancy and empty site, and thus the number of such states increases relatively slowly with N. In contrast, the conduction-band states originate from all the VB functions with non-nearest-neighbor particle and hole, and their number increases rapidly with chain length N. This is what gives a relatively large width for the conduction band in long chains. From all of the above we therefore see that it is basically possible to describe a delocalized conduction band in terms of localized valence bond functions, and, even more importantly, determine the conduction-band threshold state within the extended Hubbard model. It should also be emphasized that the only difference between the nearest-neighbor Coulomb interaction model, and models with longer-range intersite interaction, is only quantitative. Corresponding to each potential there are states with bounded double occupancy and empty site, and states with unbounded (or free) ones. The only difference between the two cases would be in the numerical magnitude of n for a given N, but in all cases n can still be determined from the same considerations as in this paper.

APPENDIX B: CANCELLATION OF TWO-PHOTON RESONANCE DUE TO $2A_g$

In Sec. III, we gave a qualitative argument as to why A_g states below the $1B_u$ will not be seen in electroabsorption. In Sec. IV, we similarly argued that these states also will not be observable in THG. The calculated electroabsorption spectra do not show any signature of these states. Within the interacting Hamiltonian, the reason behind these are the same. Each A_g state is coupled to two B_u states, and there are four possible nonlinear optical channels involving these three states. Two of these contribute to the direct terms and the other two to the cross terms in the expression of $\chi^{(3)}$. If the natures of the two B_u states (exciton, bandlike, etc.) in question are the same, and if the gaps between them are small or vanishing in the infinite chain, the direct and cross terms cancel. In this appendix, we present a more quantitative treatment. Since the argument is the same for both electroabsorption and THG, we will focus only on THG.

Because exact cancellations will not occur in finite chains, we therefore take the following approach. Since the cancellation is exact in the infinite noninteracting chain, we will compare the *tendency* toward cancellation in finite interacting and noninteracting chains. If the tendency to cancellation in the interacting short chain is comparable to or larger than that in the noninteracting chain of the same length, we can safely assume that a near cancellation will occur in the infinite interacting chain. As an example, we will consider only the $2A_g$, as the argument is equally valid for all nonessential A_g states. For the $2A_g$, one of the two relevant B_u states is the $1B_u$ exciton, the other a higher B_u state. We define two quantities P^+ and P^-, corresponding to the four-dipole products in the direct and cross terms, respectively, as follows:

$$\begin{aligned} P^+ = &\langle 1A_g|\mu|1B_u\rangle\langle 1B_u|\mu|2A_g\rangle \\ &\times\langle 2A_g|\mu|1B_u\rangle\langle 1B_u|\mu|1A_g\rangle \\ &+\langle 1A_g|\mu|jB_u\rangle\langle jB_u|\mu|2A_g\rangle \\ &\times\langle 2A_g|\mu|jB_u\rangle\langle jB_u|\mu|1A_g\rangle , \end{aligned} \tag{B1}$$

$$\begin{aligned} P^- = &\langle 1A_g|\mu|1B_u\rangle\langle 1B_u|\mu|2A_g\rangle \\ &\times\langle 2A_g|\mu|jB_u\rangle\langle jB_u|\mu|1A_g\rangle \\ &+\langle 1A_g|\mu|jB_u\rangle\langle jB_u|\mu|2A_g\rangle \\ &\times\langle 2A_g|\mu|1B_u\rangle\langle 1B_u\rangle|\mu|1A_g\rangle . \end{aligned} \tag{B2}$$

In the above, jB_u is the unique B_u state that is higher in energy than the $2A_g$ and that is strongly dipole coupled to it. We neglect the various energy denominators, as we are dealing with finite chains with discrete spectra. This is justified as long as (a) the quantum number j remains small, as in the noninteracting model; and (b) for given U, V, N and δ, j corresponds to an exciton state. In Table VII, we present the ratios $|P^-/P^+|$ for three different N and four sets of U, V, and δ (an exact cancellation would require $|P^-/P^+|=1$). In each case we have also included j. Notice that even in the interacting cases the relevant higher-energy B_u state is the $2B_u$ independent of N. For the noninteracting case a very large dimerization was chosen in order (a) to have the optical gap as large as in the interacting cases, and (b) to have the largest possible $|P^-/P^+|$. We find that for all U, V, N, and δ, the tendency to cancellation, as measured by this ratio, actually increases when Coulomb interactions are included. This indicates that the cancellation will be nearly com-

TABLE VII. The ratio $|P^-/P^+|$ for various parameters.

			$\lvert P^-/P^+\rvert$		
U	V	δ	$N=4$	$N=6$	$N=8$
0	0	0.4	0.701	0.788[a]	0.852
3	1	0.1	0.843	0.773	0.850
4	1.5	0.1	0.985	0.969	0.993
10	3	0.1	0.997	0.988	0.879[b]

[a]The jB_u is the $3B_u$ in this case, while it is $2B_u$ in all the other cases.

[b]Here the $2A_g$ is coupled to two higher B_u exciton states, $j=2$ and 3. If both are included, the total $|P^-/P^+|=0.99$.

plete in long chains, and any small nonzero contribution to THG or electroabsorption has to come from the energy difference between the $2B_u$ and the $1B_u$. Since the conduction-band threshold state is always higher than the $2B_u$, the latter is a low-energy exciton, and we conclude that the $2A_g$ will not be seen in these experiments. We have verified from exact numerical calculations that this argument remains valid for all nonessential A_g states.

The physical reason why this cancellation does not occur for the mA_g has already been discussed in Secs. III and IV. Specifically, the two B_u states coupled to the mA_g are of different nature (exciton vs band) and are separated by a gap. One could also define P^+ and P^- in this case. We have verified that in all cases the ratio P^-/P^+ decreases rapidly for increasing Coulomb interactions, reaching values as small as 0.1–0.2. Taking into account the nonzero energy gap between the $1B_u$ and the nB_u, non-negligible participation by the mA_g in nonlinear optical processes is guaranteed.

*Permanent address: Central Research Laboratories, Idemitsu Kosan Co. Ltd., 1280 Kamiizumi, Sodegaura, Chiba 299-02, Japan.

[1]*Nonlinear Optical Effects in Organic Polymers,* edited by J. Messier, F. Kajzar, P. Prasad, and D. Ulrich, Vol. 162 of *NATO Advanced Study Institute, Series E: Applied Sciences* (Kluwer, Dordrecht, 1989).

[2]*Nonlinear Optical Properties of Organic Molecules and Crystals,* edited by D. S. Chemla and J. Zyss (Academic, New York, 1987).

[3]*Proceedings of the International Conference on Optical Properties of Conjugated Polymers, Snowbird, Utah, 1991,* edited by Z. V. Vardeny and G. L. Baker [Synth. Met. **49**, 1 (1992); **50**, 367 (1992)].

[4]Author, in *Electrical, Magnetic and Optical Properties of Organic Solid State Materials,* edited by L. Y. Chiang, A. F. Garito, and D. J. Sandman, MRS Symposia Proceedings No. 247 (Materials Research Society, Pittsburgh, 1991).

[5]P. D. Townsend, G. L. Baker, N. E. Schlotter, C. F. Klausner, and S. Etemad, Appl. Phys. Lett. **53**, 1782 (1988).

[6]V. Williams, Z. Z. Ho, N. Peyghambarian, W. M. Gibbons, R. P. Grasso, M. K. O'Brien, P. J. Shannon, and S. T. Sun, Appl. Phys. Lett. **57**, 2399 (1990).

[7]M. Thakur and D. M. Krol, Appl. Phys. Lett. **53**, 1782 (1988).

[8]K. W. DeLong, K. B. Rochford, and G. I. Stegeman, Appl. Phys. Lett. **55**, 1823 (1989).

[9]G. I. Stegeman, W. Torruellas, K. B. Rochford, R. Zanoni, W. Krug, E. Miao, and M. W. Beranek, in *Proceedings of Materials Research Society Spring Meeting, Anaheim, CA, 1991,* edited by C. Warde, J. Stamatoff, and W. I. Wang, MRS Symposia Proceedings No. 228 (Materials Research Society, Pittsburgh, 1991).

[10]F. Kajzar and J. Messier, Thin Solid Films **132**, 11 (1985).

[11]W. S. Fann, S. Benson, J. M. J. Madey, S. Etemad, G. L. Baker, and F. Kajzar, Phys. Rev. Lett. **62**, 1492 (1989).

[12]W. E. Torruellas, D. Neher, R. Zanoni, G. I. Stegeman, F. Kajzar, and M. Leclerc, Chem. Phys. Lett. **175**, 11 (1990).

[13]T. Kanetake, K. Ishikawa, T. Hasegawa, T. Koda, K. Takeda, M. Hasegawa, K. Kubodera, and H. Kobayashi, Appl. Phys. Lett. **54**, 2287 (1989).

[14]J. B. van Beek, F. Kajzar, and A. C. Albrecht, J. Chem. Phys. **95**, 6400 (1991).

[15]R. R. Chance, M. L. Shand, C. Hogg, and R. Silbey, Phys. Rev. B **22**, 3540 (1980).

[16]M. L. Shand and R. R. Chance, in *Nonlinear Optical Properties of Organic and Polymeric Materials,* edited by D. J. Williams, ACS Symposia Series No. 233 (American Chemical Society, Washington, D.C., 1983).

[17]J. Le Moigne, A. Thierry, P. A. Chollet, F. Kajzar, and J. Messier, J. Chem. Phys. **88**, 6647 (1988).

[18]P. A. Chollet, F. Kajzar, and J. Messier, in *Polydiacetylenes,* edited by D. Bloor and R. R. Chance, Vol. 102 of *NATO Advanced Study Institute, Series E: Applied Sciences* (Martinus Nijhoff, Dordrecht, 1985), pp. 317–324.

[19]J. R. Heflin, K. Y. Wong, O. Zamani-Khamiri, and A. F. Garito, Phys. Rev. B **38**, 1573 (1988).

[20]Z. G. Soos, P. C. M. McWilliams, and G. W. Hayden, Chem. Phys. Lett. **171**, 14 (1990); P. C. M. McWilliams, G. W. Hayden, and Z. G. Soos, Phys. Rev. B **43**, 9777 (1991).

[21]S. N. Dixit, Dandan Guo, and S. Mazumdar, Phys. Rev. B **43**, 6781 (1991); S. Mazumdar, Dandan Guo, and S. N. Dixit, in *Photochemistry and Photoelectrochemistry of Organic and Inorganic Molecular Thin Films,* edited by M. F. Lawrence, A. J. Frank, S. Ramasesha, and C. C. Wamser, SPIE Conference Proceedings No. 1436 (International Society of Optical Engineers, Los Angeles, 1991), p. 136.

[22]S. Mazumdar, D. Guo, and S. N. Dixit, J. Chem. Phys. **96**, 6862 (1992).

[23]L. Sebastian and G. Weiser, Phys. Rev. Lett. **46**, 1156 (1981).

[24]L. Sebastian and G. Weiser, Chem. Phys. **62**, 447 (1981).

[25]Y. Tokura, Y. Oowaki, T. Koda, and R. H. Baughman, Chem. Phys. **88**, 437 (1984).

[26]Y. Tokura, T. Koda, A. Itsubo, M. Miyabayashi, K. Okuhara, and A. Ueda, J. Chem. Phys. **85**, 99 (1986).

[27]T. Hasegawa, K. Ishikawa, T. Koda, K. Takeda, H. Kobayashi, and K. Kubodera, Synth. Met. **41-43**, 3151 (1991).

[28]S. D. Phillips, R. Worland, G. Yu, T. Hagler, R. Freedman, Y. Cao, V. Yoon, J. Chiang, W. C. Walker, and A. J. Heeger, Phys. Rev. B **40**, 9751 (1989).

[29]S. Jeglinski and Z. V. Vardeny, in *Proceedings of the International Conference on Optical Properties of Conjugated Polymers, Snowbird, Utah, 1991* (Ref. 3) [Synth. Met. **50**, 509 (1992)].

[30](a) Y. Kawabe, F. Jarka, N. Peyghambarian, D. Guo, S. Mazumdar, S. N. Dixit, and F. Kajzar, Phys. Rev. B **44**, 6350 (1991); (b) *Proceedings of the International Conference on Optical Properties of Conjugated Polymers, Snowbird, Utah, 1991* (Ref. 3) [Synth. Met. **50**, 517 (1992)]. A discussion of the three-photon resonance due to the conduction-band threshold in THG experiments was given here.

[31]H. Tachibana, Y. Kawabata, S. Kosihara, and Y. Tokura, Solid State Commun. **75**, 5 (1990).

[32]R. G. Kepler and Z. G. Soos, Phys. Rev. B **43**, 12 530 (1991).

[33]D. Baeriswyl, D. K. Campbell, and S. Mazumdar, in *Conjugated Conducting Polymers,* edited by H. Kiess (Springer-Verlag, Berlin, 1992), pp. 7–133.

[34]F. Y. Guo and S. Mazumdar (unpublished).

[35]J. Le Moigne, A. Thierry, and F. Kajzar, in *Thin Films in Op-*

tics, edited by T. Tschudi, SPIE Conference Proceedings No. 1125 (International Society of Optical Engineering, Bellingham, WA, 1989), p. 9.

[36]W. P. Su, J. R. Schrieffer, and A. J. Heeger, Phys. Rev. B **22**, 2099 (1980).

[37]B. S. Hudson, B. E. Kohler, and K. S. Schulten, in *Excited States,* edited by E. C. Lim (Academic, New York, 1982), Vol. 6, pp. 1–96; B. E. Kohler and D. E. Schilke, J. Chem. Phys. **86**, 5214 (1987) find the $2A_g$ below the $1B_u$ in a polydiacetylene oligomer.

[38]Z. Shuai and J. L. Brédas, Phys. Rev. B **44**, 5962 (1991).

[39]J. Yu, B. Friedman, P. R. Baldwin, and W. P. Su, Phys. Rev. B **39**, 12 814 (1989).

[40]D. Guo, S. Mazumdar, G. I. Stegeman, M. Cha, D. Neher, S. Aramaki, W. Torruellas, and R. Zanoni, in *Electric, Magnetic and Optical Properties of Organic Solid State Materials* (Ref. 4), p. 151.

[41]Dandan Guo, S. Mazumdar, and S. N. Dixit, J. Nonlinear Opt. (to be published).

[42]S. Mazumdar, F. Guo, D. Guo, K. C. Ung, and J. Tinka Gammel, in *Proceedings of Discussion Meeting on Strongly Correlated Electron Systems in Chemistry, Bangalore, India* (Springer-Verlag, New Delhi, in press).

[43]K. C. Yee and R. R. Chance, J. Polym. Sci., Polym. Phys. Ed. **16**, 431 (1978).

[44]D. N. Batchelder, in *Polydiacetylenes* (Ref. 18), pp. 187–212, and references therein.

[45]D. Haarer and M. R. Philpott, in *Spectroscopy and Excitation Dynamics of Condensed Molecular Systems,* edited by V. M. Agranovich and R. M. Hochstrasser (North-Holland, Amsterdam, 1983), pp. 27–82.

[46]For a recent review of electroabsorption in conventional semiconductors, see N. Peyghambarian, S. W. Koch, and A. Mysyrowcyz, *Introduction to Semiconductor Optics* (Prentice-Hall, Englewood Cliffs, NJ 1993), and references therein; see also D. E. Aspnes and J. F. Rowe, Phys. Rev. B **5**, 4022 (1972); D. E. Aspnes, Phys. Rev. **153**, 972 (1967).

[47]D. Guo, S. Mazumdar, and S. N. Dixit, in *Proceedings of the International Conference on Optical Properties of Conjugated Polymers, Snowbird, Utah, 1991* (Ref. 3) [Synth. Met. **49**, 1 (1992)].

[48](a) D. Guo and S. Mazumdar, J. Chem. Phys. **97**, 2170 (1992); (b) S. Mazumdar and S. N. Dixit, Synth. Met. **28**, D463 (1989).

[49]S. Jeglinski and Z. V. Vardeny (private communication).

[50]G. Weiser and L. Sebastian, in *Polydiacetylenes* (Ref. 18), pp. 213–222; G. Weiser (private communication).

[51]S. Abe, M. Schreiber, W. P. Su , and J. Yu, Phys. Rev. B **45**, 9432 (1992).

[52]A. J. Heeger, S. Kivelson, J. R. Schrieffer, and W. P. Su, Rev. Mod. Phys. **60**, 781 (1988).

[53]M. Sinclair, D. Moses, D. McBranch, A. J. Heeger, J. Wu, and W. P. Su, Synth. Met. **28D**, 655 (1989); T. W. Hagler and A. J. Heeger, Chem. Phys. Lett. **189**, 333 (1992).

[54]M. Sinclair, D. Moses, K. Akagi, and A. J. Heeger, Phys. Rev. B **38**, 10 724 (1987).

[55]D. D. C. Bradley, N. F. Colaneri, and R. H. Friend, Synth. Met. **29E**, 121 (1989).

[56]T. Hasegawa, Y. Iwasa, H. Sunamura, T. Koda, Y. Tokura, H. Tachibana, M. Matsumoto, and S. Abe, Phys. Rev. Lett. **69**, 668 (1992).

[57]S. Mazumdar and Z. G. Soos, Synth. Met. **1**, 77 (1979).

[58]S. R. Bondeson and Z. G. Soos, J. Chem. Phys. **71**, 3807 (1979).